ACS Biomaterials SCIENCE & ENGINEERING

pubs.acs.org/journal/abseba

Article

Harnessing Hydrogel Interaction with Functional Polymeric Nanoparticles for Sustained Co-Delivery of Therapeutics

Alessandro Molinelli,† Ilaria Porello,† Francesco Briatico Vangosa, Lara Longobardi, Richard F. Loeser, Filippo Rossi,* and Francesco Cellesi*

Cite This: https://doi.org/10.1021/acsbiomaterials.6c00470

Read Online

ACCESS | Metrics & More | Article Recommendations | Supporting Information

ABSTRACT: The combination of hydrogels and polymeric nanoparticles (NPs) offers a versatile strategy to engineer multifunctional nanocomposite systems for advanced drug delivery applications. In this work, three amphiphilic block copolymers were synthesized through controlled/living polymerizations, affording macromolecules with distinct end-chain functionalities. These copolymers self-assembled into core-shell NPs, which were subsequently embedded within a cross-linked agarose-carbomer-hyaluronic acid hydrogel via physical, chemical, or ionic interactions. The incorporation of NPs within the hydrogel matrix enabled the co-delivery of both hydrophobic and hydrophilic therapeutic cargos, confining dexamethasone (DEX) in the hydrophobic NP core and a model protein within the water-rich hydrogel network. The resulting hybrid systems exhibited tunable rheological and NP release properties, depending on the NP surface moieties and the encapsulation method. Sustained DEX release was displayed over several days, and controllable protein release was achieved according to the NP surface properties. The nanocomposite showed excellent cytocompatibility, demonstrating a relevant reduction of pro-inflammatory cytokines expression *in vitro*. Overall, the proposed strategy highlights the potential of polymer chemistry-driven design to tailor hydrogel-NP interactions, providing a promising platform for targeted, sustained co-delivery of therapeutics suitable for several applications.

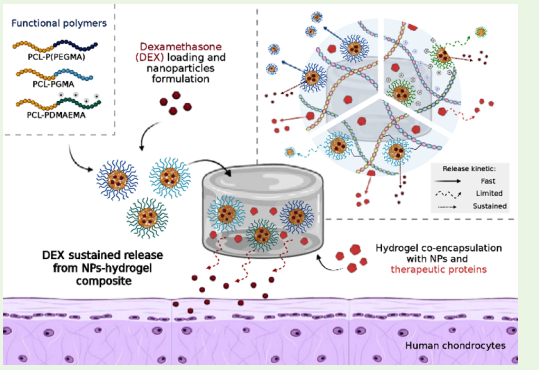

KEYWORDS: *composite hydrogel, polymeric nanoparticles, sustained drug delivery, macromolecular interactions, anti-inflammatory effect*

1. INTRODUCTION

Nanocomposite systems constituted of hydrogels and polymeric nanoparticles (NPs)[1,2] have recently emerged as highly versatile platforms for a broad spectrum of biomedical applications,[3] including drug delivery,[4,5] cancer therapy,[6] tissue engineering,[7] wound healing,[8] and gene therapy.[9] These systems combine the structural and physicochemical advantages of hydrogels with the functional versatility of NPs, creating promising polyvalent constructs[10,11] with synergistic and tunable properties, specifically engineered to overcome the intrinsic weakness of each individual component.[12] Hydrogels can be formulated from a wide range of natural or synthetic polymers and are distinguished by their remarkable ability to retain large amounts of water,[12] which confers excellent swelling capacity, biocompatibility, biodegradability, and favorable cellular interactions.[13,14] However, their pronounced hydrophilicity poses major challenges for drug delivery,[15] as most therapeutic molecules are hydrophobic, leading to poor drug solubility, drug aggregation, or uncontrolled burst release.[12,16] In addition, hydrogels generally display low mechanical strength and lack multifunctional features, which are essential for selective *in situ* delivery.[7] On the other hand, polymeric NPs are copolymer-based colloidal structures characterized by distinct hydrophilic and hydrophobic domains.[17−20] They are typically designed to cross biological barriers, protecting therapeutics from degradation while prolonging their half-life.[21] Polymeric NP surface functionalization further enables targeted delivery, thereby reducing systemic toxicity and minimizing off-target effects.[18,19] Nevertheless, NPs are frequently prone to premature clearance and burst release, with unpredictable drug retention at the target site.[21] Hybrid NPs-hydrogel composites have paved the way to overcome the aforementioned challenges, leading to overall enhanced therapeutic performances.[12,22,23] By integrating the NPs into the hydrogel matrix, the gel acts as a depot for both the NPs and the loaded active substances, reducing their rapid clearance from the site of administration and slowing drug release over time, with minimized burst release.[1,24−27] Among others, one of the most appealing features of these platforms is their

Received: March 18, 2026
Revised: May 2, 2026
Accepted: June 8, 2026

dual-compartment structure, in which NPs and the hydrogel matrix act as complementary reservoirs for therapeutic agents.[23] NPs provide a hydrophobic environment for the encapsulation of lipophilic drugs, while the water-rich hydrogel favors the incorporation of hydrophilic molecules.[28] In this way, therapeutic agents with distinct physicochemical properties (small drugs,[16] proteins,[29] growth factors,[23,30] and cytokines[31]) can be simultaneously co-delivered, and synergistic therapeutic effects can be obtained through different or complementary release rates.[6,9]

Achieving predictable *in vitro* and *in vivo* behavior requires the rational design of both the hydrogel and the NPs.[32] By carefully selecting the polymeric materials, cross-linking mechanisms and density, the hydrogel features, such as mesh size, porosity, swelling, viscoelasticity, and mechanical strength, can be finely tuned.[33] Similarly, NPs can be engineered through adjustment of their architecture, monomer composition, and hydrophilic/hydrophobic balance, yielding well-defined structures with specific functionalities.[17,18] These parameters collectively govern the interactions established within the NPs-hydrogel network that are critical in determining physicochemical properties, drug loading capacity, release kinetics, and overall biological behavior of the final composite system.[9,23,34] A variety of formulation strategies have been investigated to form these composite systems, including physical embedding through nonspecific interactions,[34] hydrophobic interactions,[35] electrostatic interactions,[36] and chemical bonding.[22] Despite the growing number of NPs-hydrogel nanocomposites reported in the literature, most of them rely on complex synthetic and post-modification routes to achieve tailored features.[18,23] In this work, a multivalent composite platform is proposed, consisting of hydrogels embedding polymeric NPs for the simultaneous co-delivery of multiple therapeutics: a hydrophobic synthetic drug encapsulated within the NP core, and a model protein entrapped within the hydrogel matrix. To this end, three distinct amphiphilic block copolymers were synthesized via ring-opening polymerization (ROP) and atom transfer radical polymerization (ATRP), yielding structures with different terminal functionalities. The proposed approach highlights that the modulation of nanocomposite properties can be effectively achieved by simply tailoring the chemistry of the hydrophilic block within a unified block copolymer design, coupled with a rational optimization of the composite formulation process. Specifically, poly(poly(ethylene glycol) methyl ether methacrylate) P(PEGMA), poly(2-(dimethylamino)ethyl methacrylate) (PDMAEMA), and poly(glycerol methacrylate) (PGMA) blocks were synthesized from poly(ε-caprolactone) (PCL)-based macroinitiators. These copolymers were designed to self-assemble in aqueous media, forming core-shell NPs capable of encapsulating dexamethasone (DEX) within their hydrophobic core, which is widely recognized for its powerful anti-inflammatory and antioxidant properties.[37−39] The NP incorporation within the hydrogel network was achieved by harnessing the interactions between the NP surface functionalities and the hydrogel constituents (Figure 1). The hydrogel was obtained through a polycondensation reaction between agarose, carbomer, and hyaluronic acid (HA). BSA was selected as a model protein to mimic the encapsulation and release of therapeutic proteins or antibodies within the hydrogel phase. The resulting composite systems were thoroughly characterized in terms of rheological behavior and release kinetics of the NPs, DEX, and BSA, proposing a comparative evaluation of how NPs-hydrogel-cargos interactions influence overall release performance. Finally, the therapeutic potential of the system was assessed *in vitro* on human chondrocyte cell cultures, given the suitability of this platform in anti-inflammatory applications. In this perspective, osteoarthritis (OA)[38,40,41] represents a particularly suitable target for the proposed system, which benefits from the synergistic DEX anti-inflammatory effect,[37,42] and the HA lubricating properties.[43,44] HA is indeed one of the major components of the synovial fluid, which provides lubrication for joints.

2. MATERIALS AND METHODS

Materials

ε-Caprolactone 97% (ε-CL), poly(ethylene glycol) methyl ether methacrylate M_n= 500 Da (PEGMA), (dimethylamino)ethyl methacrylate ≥ 98% (DMAEMA), Benzyl alcohol 99.8% anhydrous (BnOH), Rhodamine B ≥ 95% (RhB), 2-hydroxyethylmethacrylate ≥ 99%

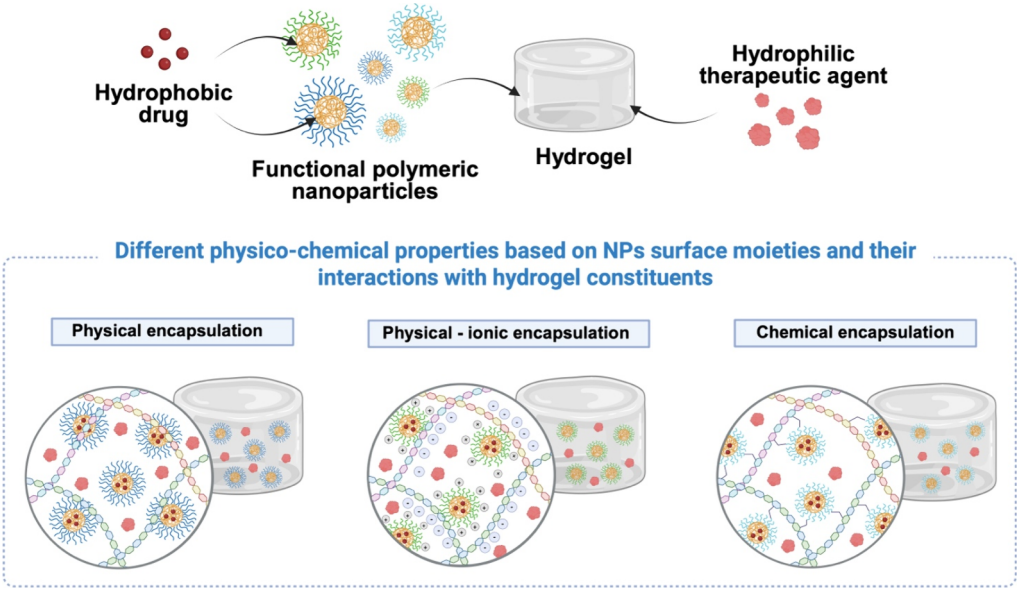

Figure 1. Schematic representation of the different physicochemical assemblies strategies employed for NPs-hydrogel composites formulation.

https://doi.org/10.1021/acsbiomaterials.6c00470
ACS Biomater. Sci. Eng. XXXX, XXX, XXX−XXX

(HEMA), *N*,*N*′-dicyclohexylcarbodiimide 99% (DCC), 4-(dimethylamino)pyridine ≥ 99% (DMAP), α-bromoisobutyryl bromide 98% (BiBB), ethyl-α-bromoisobutyrate 98% (EBiB), 2,2′-bipyridyl ≥ 99% (BPY), Tin(II) 2-ethylhexanoate 92−100% ($Sn(Oct)_2$), copper (I) bromide 98% (CuBr(I)), copper (II) chloride 97% ($CuCl_2$(II)), L-ascorbic acid 99% (AA), isopropyl alcohol ≥ 99.8% (IPA), acetonitrile (ACN), acetonitrile for HPLC gradient grade 99.9% (ACN), *N*,*N*-dimethylformamide ≥ 99.8% anhydrous (DMF), methanol ≥ 99.8% (MeOH), tetrahydrofuran ≥ 99.9% anhydrous inhibitor-free (THF), tetrahydrofuran ≥ 99.9% gel permeation chromatography grade (THF), toluene ≥ 99.9% anhydrous, dichloromethane ≥ 99.8% (DCM), diethyl ether ≥ 99.8% (Et_2O), ethyl acetate ≥ 95%, 2, dexamethasone ≥ 98% (DEX), triethylamine ≥ 99% (TEA), hydrochloric acid > 37% (HCl), 1,1,4,7,10,10-hexamethyltriethylenetetramine 97% (HMTETA), hexane ≥ 99%, deuterochloroform ≥ 99.8% ($CDCl_3$), aluminum oxide (Al_2O_3), lithium bromide 99% (LiBr), sodium bicarbonate ($NaHCO_3$), sodium sulfate ≥ 99% (Na_2SO_4), sodium chloride ≥ 99% (NaCl), sodium hydroxide pellets ≥ 97% (NaOH), and albumin-fluorescein isothiocyanate conjugate (BSA-FITC) were all purchased from Sigma-Aldrich (Merck, Italy). Dimethyl sulfoxide-d_6 100% (DMSO-d_6) and deuterium oxide 100% (D_2O) were purchased from Eurisotop (Cambridge Isotope Laboratories, France). *N*,*N*-Dimethylacetamide ≥ 99.5% (DMAc) was purchased from ThermoFisher Scientific (Italy). Glycerol monomethacrylate (GMA) was purchased from Polysciences (Germany). Tris (2-pyridylmethyl) amine (TPMA) was purchased from Tokyo Chemical Industry (Belgium). Agarose (M_n = 200 kDa) was purchased from Invitrogen (USA). Sodium hyaluronate (M_n = 10 kDa) was purchased from LifeCore (USA). Carbomer 974P (M_n = 1 kDa) was purchased from Fargon (Netherlands). Dulbecco's modified Eagle medium/Nutrient Mixture F-12 (DMEM/F-12), Fetal bovine serum (FBS), penicillin-streptomycin (P/S), gentamicin (Gent), and Dulbecco's phosphate-buffered saline sterile (DPBS) were purchased from Gibco. Amphotericin B (Amp B) was purchased from Sigma-Aldrich (USA). Molecular biology grade water was purchased from Corning. All chemicals were used without further purification unless otherwise indicated. Deionized water (18.2 MΩ) was obtained from a Millipore Milli-Q purification unit.

Polymer Characterization

Monomer conversion (χ_{ROP}, χ_{ATRP}) and polymer degree of polymerization (DP_{real}) were determined by ^{1}H NMR analysis, dissolving crude and purified polymers in the proper deuterated solvent. ^{1}H NMR spectra were recorded on a Bruker Avance 400 MHz at 298 K, using $CDCl_3$ or DMSO-d_6 as solvent. Chemical shifts (δ) are reported in ppm downfield from the deuterated solvent used as an internal standard. The polymer number-average molar mass ($M_{n,SEC}$) and dispersity ($Đ = M_w/M_n$) values were evaluated using two Jasco LC-2000Plus size exclusion chromatography (SEC) instruments, both equipped with an AS-2055Plus autosampler, a refractive index detector (RI-2031Plus, Jasco), a PU-2080 pump, and a CO-2060 plus oven column. One system employs 3× Agilent PCgel columns (300 × 7.5 mm, 5 μm particle size) and 1 × PCgel guard (50 × 7.5 mm, 5 μm particle size) using THF as eluent at 35 °C. The second SEC system works with 3 × GRAM columns (300 × 8 mm, 10 μm particle size) and 1 × GRAM guard (50 × 8 mm, 10 μm particle size) using DMAc (30 mM LiBr) as eluent at 40 °C. Both instruments were calibrated by using polystyrene standards (calibration kits by RESTEK and Sigma-Fluka). According to the compound solubility, samples of purified polymer were dissolved in THF (containing 250 ppm BHT as inhibitor) or DMAc at a concentration of 4 mg/mL, filtered through PTFE syringe filters (0.22 μm), and injected at a flow rate of 1 mL/min.

Synthesis of HEMA-RhB

1 g of RhB (2.1 mmol, 1 equiv) together with 0.325 g of HEMA (2.5 mmol, 1.2 equiv) were dissolved in 20 mL ACN under magnetic stirring at 20 °C. Meanwhile, 0.43 g of DCC (2.1 mmol, 1 equiv) and 13 mg of DMAP (106 mmol, 0.05 equiv) were dissolved in an additional 20 mL of ACN. This solution was added by means of a dropping funnel to the HEMA-RhB reacting mixture (20 min, ∼1 mL/min), leaving the system under N_2 flux. The reaction was carried out in the dark at 40 °C under magnetic stirring for 24 h. The mixture was then quenched in an ice bath for 10 min to facilitate dicyclohexylurea precipitation. This side product of the coupling reaction was eliminated from the solution through filtration, and finally, ACN was removed under reduced pressure. The collected solid was redispersed in a mixture composed of 40 mL of EtAC and 40 mL of a diluted aqueous solution of $NaHCO_3$ (0.1 M, pH ≈ 8.4). The water phase (∼40 mL) was isolated by means of a separating funnel, washed three times with fresh EtAC (1/1 v/v), and successively saturated with NaCl. The pH was maintained neutral by adding drops of a 1 M HCl solution. The product was then extracted from the aqueous phase with an organic mixture (1/1 v/v) of DCM/IPA 1:2 v/v. The organic phase was collected and dried with $NaSO_4$ while the solvent was removed by rotary evaporator. The collected solid was dissolved in a small amount of MeOH and precipitated into cold Et_2O. Yield = 80%.

Synthesis of PCL_n-b-$P(PEGMA)_m$

The reaction macroinitiator (I) PCL_n-Br (500 mg, 1 equiv) and the monomer PEGMA (30 equiv) were inserted into a Schlenk flask, and three cycles of nitrogen/vacuum of 5 min each were performed. THF (inhibitor-free) was degassed under nitrogen for 30 min. The catalyst solution (C) was prepared as follows: Cu(I)Br (574 mg) was inserted in a double-neck flask, and three cycles of vacuum/nitrogen were performed. 5 mL of degassed THF and 1 mL of the ligand (L) HMTETA were added to the system and stirred at r.t. under nitrogen for 10 min. THF was added to the reaction mixture ([PEGMA] ≤ 1 M) that was heated and kept at 50 °C until complete dissolution of the solid components. Finally, the required amount of catalyst solution ([C]/[L]/[I] = 1/1/1) was added to the monomer. The reaction mixture was stirred overnight at 50 °C. The purification was performed by filtering the crude through a neutral alumina pad (h = 3 cm, Φ = 2 cm), washing with THF. Subsequently, the filtrate was dried under reduced pressure, and the crude was dissolved in DCM (2 mg/mL) and dropped in cold Et_2O (DCM/Et_2O = 1/100 v/v), maintaining the system under stirring in an ice bath. The mixture was stored at −20 °C for 30 min, and the resulting precipitate was isolated by removing the supernatant through filtration. Yield > 80%. ^{1}H NMR (400 MHz, $CDCl_3$), δ (ppm): δ 7.34 (s, 5H, PCL: C_6H_5−CH_2−), 5.11 (s, 2H, PCL: C_6H_5−CH_2−OC(O)−), 4.14−4.02 (m, 2H·n + 4H, PCL: −CH_2−OC(O)−, PEG: −O−CH_2CH_2−O−), 3.6 (m, 4H·8·m, PEG: −CH_2CH_2−), 3.38 (s, 3H·m, PEG: −OCH_3), 2.32−2.25 (t, 2H·n, PCL: −OC(O)−CH_2−), 1.92 (s, 6H, −CH_2OC(O)C(CH_3)$_2$−), 1.48−1.65 (m, 4H·n, PCL: −OC(O)−CH_2CH_2−, −CH_2CH_2−OC(O)−), 1.25−1.38 (m, 2H·n, PCL: −$CH_2CH_2CH_2$−), 1.2−0.6 (m, 3H·m, PEG: $CH_{3,backbone}$), where n is the PCL degree of polymerization, and m is the P(PEGMA) degree of polymerization.

Synthesis of PCL_n-b-$PGMA_m$

The reaction macroinitiator (I) PCL_n-Br (500 mg, 1 equiv) and the monomer GMA (30 equiv) were weighed into a Schlenk flask, and three cycles of nitrogen/vacuum of 5 min each were performed. DMF was degassed under nitrogen for 30 min. The catalyst solution (C) was prepared as follows: $CuCl_2$ (107 mg) and the ligand (L) TPMA (465 mg) were added in a double-neck flask, and three cycles of vacuum/nitrogen were performed. 2 mL of degassed DMF was added, mixing at r.t. under nitrogen for 10 min. The reducing agent (R) solution was obtained by inserting AA (528 mg) in a double-neck flask and performing three cycles of vacuum/nitrogen prior to the addition of 2 mL of DMF. DMF was added to the reaction mixture ([GMA] ≤ 1 M), and the flask was heated up to 50 °C until complete dissolution of the solid components. Finally, the catalyst solution ([C]/[L]/[I] = 1/2/1) and the AA solution ([C]/[L]/[R] = 1/2/5) were added to the monomers. The reaction mixture was stirred

https://doi.org/10.1021/acsbiomaterials.6c00470
ACS Biomater. Sci. Eng. XXXX, XXX, XXX−XXX

overnight at 50 °C. The purification was performed by filtering the crude mixture through a neutral alumina pad (h = 3 cm, Φ = 2 cm), washing with THF. Then the filtrate was dried under reduced pressure, and the crude was dissolved in the minimum amount of DCM (2 mg/mL) and dropped in cold IPA (DCM/IPA = 1/100 v/v), maintaining the system under stirring in an ice bath. The mixture was stored at −20 °C, and the resulting precipitate was isolated by removing the supernatant through filtration. Yield 60–70%. ^{1}H NMR (400 MHz, DMSO-d_6), δ (ppm): *δ* 4.89–4.65 (s, 2H·*m*, GMA: −CH_2−OH, −CH−OH), 3.99 (t, 2H·*n-1*, PCL: −CH_2−OC(O)−), 3.85–3.6 (m, 3H·*m*, GMA: −O−CH_2−CH(OH)−), 3.39 (s, 2H·*m*, GMA: −CH−CH_2−OH), 2.27 (t, 2H·*n*, PCL: −OC(O)−CH_2−), 1.92 (s, 6H, −CH_2OC(O)C(CH_3)$_2$−), 1.63–1.48 (m, 4H·*n*, PCL: −OC(O)−CH_2CH_2−, −CH_2CH_2−OC(O)−), 1.37–1.25 (m, 2H·*n*, PCL: −$CH_2CH_2CH_2$−), 1.2–0.6 (m, 3H·*m*, GMA: $CH_{3,backbone}$), where *n* is PCL degree of polymerization, *m* is PGMA degree of polymerization.

Synthesis of PCL_n-b-$PDMAEMA_m$

The reaction macroinitiator (I) PCL_n-Br (500 mg, 1 equiv) and the monomer DMAEMA (30 equiv) were added to a Schlenk flask, and three cycles of nitrogen/vacuum of 5 min each were performed. THF (inhibitor-free) was degassed under nitrogen for 30 min. The catalyst solution (C) was prepared as follows: CuBr (574 mg) and the ligand (L) BPY (864 mg) were inserted in a double-neck flask, and three cycles of vacuum/nitrogen were performed. 2 mL of degassed THF was added, and the mixture was stirred at r.t. under nitrogen for 10 min. THF was added to the reaction mixture ([DMAEMA] ≤ 1 M), and the flask was heated up to 50 °C until complete dissolution of the solid components. Finally, the catalyst solution ([C]/[L]/[I] = 1/2/1) was added to the monomer. The reaction mixture was stirred overnight at 30 °C. The purification was performed by filtering the crude mixture through a silica pad (h = 3 cm, Φ = 2 cm), washing with DMC. Then, the filtrate was dried under reduced pressure, and the crude was dissolved in DCM (2 mg/mL) and dropped in cold hexane (DCM/hexane = 1/100 v/v), maintaining the system under stirring in an ice bath. The mixture was stored at −20 °C for 30 min, and the resulting precipitate was isolated by removing the supernatant through filtration. Yield > 90%. ^{1}H NMR (400 MHz, $CDCl_3$), δ (ppm): δ 7.34 (s, 5H, PCL: C_6H_5−CH_2−), 5.11 (s, 2H, PCL: C_6H_5−CH_2−OC(O)−), 4.14–4.02 (m, 2H·*n* + 2H·*m*, PCL: −CH_2−OC(O)−, PDMAEMA: −O−CH_2−),3.10–3.20 (m, 2H·*m*, PDMAEMA: −OCH_2CH_2N−), 2.32–2.25 (t, 2H·*n*, PCL: −OC(O)−CH_2−), 2.30–2.20 (s, 6H·*m*, PDMAEMA: −N(CH_3)$_2$−), 1.92 (s, 6H, −CH_2OC(O)C(CH_3)$_2$−), 1.48–1.65 (m, 4H·*n*, PCL: −OC(O)−CH_2CH_2−, −CH_2CH_2−OC(O)−), 1.25–1.38 (m, 2H·*n*, PCL: −$CH_2CH_2CH_2$−), 1.2–0.6 (m, 3H·*m*, PDMAEMA: $CH_{3,backbone}$), where *n* is PCL degree of polymerization, *m* is PDMAEMA degree of polymerization.

For PCL_n-P(PEGMA)$_m$, PCL_n-$PGMA_m$, and PCL_n-$PDMAEMA_m$ polymers, the syntheses described above were also carried out by incorporating HEMA-RhB as a co-monomer along with the corresponding hydrophilic monomer (PEGMA, GMA, or DMAEMA) during ATRP. HEMA-RhB was used at a 1:100 molar ratio relative to the hydrophilic monomer, in order to obtain fluorescently labeled polymers analogous to the native ones and showing the same design parameters.

Nanoparticles Formulation

NPs were prepared according to a nanoprecipitation/solvent evaporation method.[17,18] Briefly, from 1 to 20 mg of copolymer were dissolved under stirring in 1 mL of acetone. The solution was added dropwise into 1 mL of PBS (10 mM, pH 7.4) or ultrapure water and stirred for 10 min. Acetone was removed at the rotary evaporator under controlled gradient of pressure (from 1000 mbar to 100 mbar in 1 h, and then setting it at 100 mbar for 1 h) at 30 °C. Particle size distribution, average size (Z-Av.), polydispersity index (PdI) (1 mg/mL in ultrapure water), and ζ-potential (ζ-pot.) (0.5 mg/mL in ultrapure water) were evaluated at 25 °C via dynamic light scattering (DLS) using a Malvern Zetasizer Ultra, equipped with a 4 mW He−Ne laser operating at λ = 632.8 nm (backscattered angle 173°).

Preparation of Drug-Loaded NPs

2 mg of dexamethasone (DEX) was dissolved in 1 mL of acetone together with 20 mg of copolymer. The mixture was stirred for 15 min and then added dropwise into 1 mL of ultrapure water or PBS (10 mM, pH 7.4). The mixture was stirred for 15 min, and acetone was removed at the rotary evaporator under a controlled gradient of pressure (from 1000 mbar to 100 mbar in 1 h, and then setting it for 1 h at 100 mbar) at 30 °C. To remove the unloaded DEX from the NP suspension, the latter was filtered using 0.22 μm PTFE filters. The amount of DEX encapsulated in the polymeric nanocarriers was determined by using an HPLC system (Jasco) equipped with a Restek C18 column and a photodiode array PDA detector. Detector wavelength was set at 270 nm, the mobile phase was composed of ACN and ultrapure water (52/48 v/v) in isocratic conditions at a flow rate of 1 mL/min at 25 °C. 200 μL of DEX-loaded NP suspension was lyophilized using a Modulyo EF4-1596 freeze-dryer (Edwards). Subsequently, 200 μL of DMSO was added to dissolve the and release the encapsulated DEX for quantification. The encapsulation efficiency (EE) and drug loading (DL) were calculated as reported in eqs 1 and 2, determining the amount [mg] of DEX loaded by means of a calibration curve obtained by dissolving the pure drug in DMSO (Figure S1, Supporting Information).

$$\mathrm{DL} = \frac{\text{mass DEX loaded [mg]}}{\text{mass solid phase [mg]}}\,\% \tag{1}$$

Drug loading (DL) and encapsulation efficiency (EE) evaluation for DEX-loaded NPs.

$$\mathrm{EE} = \frac{\text{mass DEX loaded [mg]}}{\text{mass DEX feed [mg]}}\,\% \tag{2}$$

Encapsulation efficiency (EE) evaluation for DEX-loaded NPs.

DEX-loaded NPs were analyzed at DLS for a comparison of the particles size distribution and average size with the ones obtained before DEX loading.

DEX Release from NPs

3 mL of each DEX-loaded NP suspension was formulated at 5 mg/mL, as previously described, and was placed in a Spectra Por 1 kDa MWCO dialysis membrane closed with tubing clips. The membranes were placed in Falcon tubes containing 40 mL of PBS at 37 °C for the release test. 1 mL of PBS was withdrawn at specific time points, and it was substituted with freshly added PBS. The withdrawn aliquots were freeze-dried (Modulyo EF4-1596 freeze-dryer, Edwards), redispersed in 200 μL of DMSO, and then filtered to remove salt residues. The amount of DEX released at each time point was evaluated by using the Jasco HPLC machinery previously described, equipped with a Restek C18 column. The detector wavelength was set at 270 nm, the mobile phase was composed of ACN and ultrapure water (52/48 v/v) in isocratic conditions at a flow rate of 1 mL/min at 25 °C. The drug cumulative release [%] was calculated by determining the amount [mg] of DEX released by means of a calibration curve obtained by dissolving the pure drug in DMSO (Figure S1) as performed for EE and DL evaluation. The release profiles obtained were fitted with the Korsmeyer-Peppas (KP) and Peppas-Sahlin (PS) diffusion models according to eqs 3 and 4.

$$\frac{M_t}{M} = K_1 \times t^n \tag{3}$$

The Korsmeyer-Peppas model is used for describing the fraction of drug released as a function of time, where t is the time, M_t is the

https://doi.org/10.1021/acsbiomaterials.6c00470
ACS Biomater. Sci. Eng. XXXX, XXX, XXX−XXX

cumulative mass released at time t, M_∞ is the total mass of drug released at $t = \infty$, K_1 is the coefficient describing diffusional contribution, and n is the diffusional exponent.

$$\frac{M_t}{M} = K_1 \times t^n + K_2 \times t^{2n} \quad (4)$$

The Peppas-Sahlin model is used for describing the fraction of drug released as function of time, where t is the time, M_t is the cumulative mass released at time t, M_∞ the total mass of drug released at $t = \infty$, K_1 is the coefficient describing diffusional contribution, K_2 is the coefficient describing the contribution of polymer relaxation, n is the diffusional exponent, and $2n$ is the temporal growth of the relaxation contribution.

Pristine AC-HA Hydrogels Formulation

The hydrogel synthesis was adapted from a previously existing protocol with some modifications.[43] Briefly, the polymer solution was obtained by dissolving carbomer 974P and sodium hyaluronate in PBS under continuous stirring at room temperature, with a final concentration of 1.6 and 17.5 mg/mL, respectively. The pH of the solution was adjusted to 7.4 with 1 M NaOH solution. The AC-HA hydrogel was achieved by dissolving agarose in the polymer solution (at a concentration of 5 mg/mL), using 500 W electromagnetic stimulation heating at 80 °C. The reaction time was dependent on the reactive volume, i.e., 1 min per 10 mL of polymeric solution. Then, before reaching the sol-gel transition temperature (~45 °C), the solution was diluted in a 1:1 v/v ratio with either 2 mg/mL BSA-FITC solution for BSA-encapsulated hydrogels or PBS for the pristine samples. The sol-gel transition process was carried out in 1 cm-diameter cylindrical-shaped molds with a final volume of 0.5 mL.

IR Spectroscopy Analysis

Infrared (IR) spectra of the hydrogels were acquired with an Agilent Cary 630 spectrometer from Agilent Technologies. The spectra were recorded in the 650–4000 cm^{-1} range at a 4 cm^{-1} resolution and 64 scans/spectra under dry nitrogen conditions. The spectra were processed and reported with baseline correction and reversed y-axis.

NPs-Hydrogel Composites Formulation

NPs-hydrogel composites were formulated using the same protocol employed for AC-HA hydrogel preparation, with some modification according to NP shell functionality.

For the case of physical and ionic NP encapsulation (with PCL-P(PEGMA) and PCL-PDMAEMA polymers), the hydrogel was synthesized by dissolving agarose (at a concentration of 5 mg/mL) in the pristine polymer solution, by means of a 500 W electromagnetic stimulation heating at 80 °C. Before reaching the sol-gel transition temperature (~45 °C), the solution was diluted in a 1:1 v/v ratio with the respective NP solution (20 mg/mL in PBS), or with a mix of the NP solution and BSA-FITC, to reach a final NP concentration of 10 mg/mL in each hydrogel.

For the case of NP chemical loading (using PCL-PGMA polymer), carbomer 974P and sodium hyaluronate were dissolved by gentle stirring in 3 mL of 20 mg/mL NP solution in PBS at r.t., with final concentrations of the polymers at 1.6 and 17.5 mg/mL, respectively. After complete dissolution, 15 mg of agarose (to reach a final concentration of 5 mg/mL) was dissolved in the previously obtained solution by means of a 500 W electromagnetic stimulation heating at 80 °C for 2 min. Before the sol-gel transition took place (~45 °C), the solution was diluted in a 1:1 v/v ratio with either PBS or 2 mg/mL BSA-FITC solution in PBS.

SEM Analysis

Scanning electron microscopy (SEM) analysis of pristine hydrogels and NP-loaded hydrogels was carried out on gold sputtered cylindrical-shaped (1 cm diameter, 0.5 mL volume) dry samples to determine the internal morphology of the hydrogel using a Zeiss Evo50 with EDS Bruker Quantax 200 microscope. The samples were formulated as reported above and immediately frozen at −80 °C, and then freeze-dried for the analysis.

AC-HA and NPs-Hydrogel Rheological Characterization

Pristine AC-HA and NP-loaded hydrogels were formulated as previously reported, with a final volume of 1 mL into 10 mm diameter cylindrical shape molds for rheological properties investigation. Oscillatory rheological measurements were performed at 25 °C with an Anton Paar MCR 502 rheometer equipped with a parallel plate measuring system (diameter = 25 mm, plate-plate distance = 1 mm). Amplitude sweep tests were carried out to determine the linear viscoelastic (LVE) region limit, varying the shear strain amplitude according to a logarithmic ramp ranging from 0.01% to 100 % at a fixed frequency of 10 rad/s. Frequency sweep tests were performed to characterize the viscoelastic behavior of the hydrogel within the linear range (shear strain 0.3%, evaluated through amplitude sweep tests) by frequency variation with a logarithmic ramp between 0.1 and 100 rad/s.

NP Release from NPs-Hydrogels

NPs-hydrogels (0.5 mL volume, 1 cm diameter) were formulated with the three different NP suspensions at a fixed NP concentration (10 mg/mL) as previously described. Successively, they were inserted into a Corning 24 multiwell plate, covered with 2 mL of PBS (10 mM, pH 7.4), and incubated at 37 °C to simulate *in vitro* release conditions. 1 mL of PBS release medium was withdrawn at specific time points and replaced with the same volume of fresh PBS. The withdrawn samples were analyzed both via UV-vis spectroscopy (Jasco-630 UV-vis spectrophotometer) and via DLS using a Malvern Zetasizer Nano ZS, equipped with a 4 mW He–Ne laser operating at λ = 632.8 nm (backscattered angle 173°).

UV-vis analysis was employed to quantify the amount of NPs released at each time point, exploiting the presence of RhB in their shell. Measurements were performed at λ = 564 nm, corresponding to the RhB maximum absorption peak. The cumulative NP release [%] was calculated as described in eq 3 by determining the amount of NPs released [mg] through a calibration curve, established according to the Lambert-Beer law, which relates the recorded absorbance to the analyte concentration. This curve was obtained by diluting RhB-labeled NPs in PBS at different known concentrations (Figure S2, Supporting Information).

In parallel, DLS analysis was carried out, recording the samples derived count rate (attenuator = 8, measurement position = 3). As in the UV-vis analysis, the NP cumulative release was quantified using a calibration curve obtained by diluting the NPs in PBS at various known concentrations and correlating it with the measured count rate (Figure S4, Supporting Information). The release profiles obtained were fitted with the KP and PS diffusion models according to eqs 3 and 4, respectively, analogous to the case of DEX release from the NPs.

DEX Release from NPs-Hydrogels

NPs-hydrogels were formulated with the three different DEX-loaded NP dispersions at 10 mg/mL, as previously described. The hydrogels were molded in cylindrical shapes (0.5 mL volume, 1 cm diameter) and were placed in 1 kDa MWCO Spectra/Por dialysis membranes, closed with tubing clips with 3 mL of PBS. Each membrane was inserted in Falcon conical tubes containing 40 mL of PBS at 37 °C for the release test for 21 days. 1 mL of PBS was withdrawn at specific time intervals, and it was substituted with freshly added PBS. The withdrawn aliquots were freeze-dried, then redispersed in 200 μL of DMSO, and filtered to remove salt residues. The amount of DEX released at each time point was evaluated by using the Jasco HPLC machinery previously described, equipped with a Restek C18 column. The detector wavelength was set at 270 nm, the mobile phase was composed of ACN and ultrapure water (52/48 v/v) in isocratic conditions at a flow rate of 1 mL/min at 25 °C. The drug cumulative release

https://doi.org/10.1021/acsbiomaterials.6c00470
ACS Biomater. Sci. Eng. XXXX, XXX, XXX–XXX

[%] was calculated by determining the amount [mg] of DEX released by means of a calibration curve obtained by dissolving the pure drug in DMSO. The release profiles obtained were fitted with the KP and PS diffusion models according to eqs 3 and 4, respectively, analogous to the previous cases.

BSA Release from NPs-Hydrogels

NPs-hydrogels were formulated as previously described with a fixed concentration of NPs (10 mg/mL) and 1 mg/mL BSA-FITC and were placed in Corning 24 multiwell plates covered with 2 mL of PBS at 37 °C. At specific time points, 1 mL of PBS release medium was withdrawn and substituted with fresh PBS. The withdrawn samples were analyzed by means of UV-vis absorbance using a UV-vis spectrophotometer (Jasco-630) at a fixed wavelength (λ = 495 nm) corresponding to the FITC absorption peak. The BSA-FITC cumulative release [%] was calculated by determining the amount [mg] of BSA released through a calibration curve, established according to the Lambert-Beer law, which relates the recorded absorbance to the analyte concentration. The calibration curve was obtained by dissolving pure BSA-FITC in PBS at different concentrations (Figure S4, Supporting Information). The release profiles obtained were fitted with the KP and PS diffusion models according to eqs 3 and 4, respectively, analogous to the previous cases.

Human Chondrocytes Isolation and Culture

Primary articular chondrocytes were isolated by enzymatic digestion from normal human femoral cartilage obtained through the Gift of Hope Organ and Tissue Donor Network (Itasca, IL), as previously described.[45,46] The tissue was obtained from donors with a lack of morphological indications of osteoarthritis as determined by the Collin's score.[47] Only normal cartilage was used, avoiding areas with signs of degeneration. Cells were cultured to 80−90% confluency in DMEM/F-12 media with 10% FBS with the addition of P/S, Gent, and Amp B as antibiotics before any treatment. Use of human tissue in agreement with both Rush University Medical Center and the University of North Carolina at Chapel Hill Institutional Review Boards.

Cell Viability Assay

Cells were cultured in Corning 96-well plates at 75 k cells/well in DMEM/F-12 with 10% FBS from 24 to 48 h. Afterward, the media was removed, and cells were treated with either PCL-P(PEGMA), PCL-PGMA, or PCL-PDMAEMA NPs premixed with AC-HA solution and then diluted in DMEM/F-12 media with 10% FBS in a concentration window ranging from 100 to 1 μM of NPs. Additionally, some wells were treated with free DEX dissolved in DMEM/F-12 with 10% FBS (with 0.1% v/v DMSO), while controls were treated either with DMEM/F-12 with 10% FBS (100% live) or 70% MeOH (100% dead). After 24 h of treatment, the media were removed, and the cells were thoroughly washed with PBS. Cells were treated with LIVE/DEAD Viability/Cytotoxicity Kit for mammalian cells (L3224, Invitrogen) as described in the kit protocol and incubated for 30 min. The number of live and dead cells was determined by counting the number of Calcein AM and ethidium homodimer-1-stained cells from fluorescence microscopy acquisitions, obtained using an EVOS M5000 microscope equipped with an EVOS Olympus 4× objective (AMEP4752). The images were acquired with the GFP (green) channel ($\lambda_{ex}/\lambda_{em}$ = 470/525 nm) and RFP (red) channel ($\lambda_{ex}/\lambda_{em}$ = 531/593 nm) and processed using ImageJ. The number of alive cells was determined with eq 5.

$$\%\text{Live} = \frac{\text{Number of alive cells}}{\text{Number of alive cells} + \text{Number of dead cells}} \times 100 \quad (5)$$

Evaluation of alive cell % after 24 h from NP administration.

Measurement of Inflammation Factors in Human Chondrocytes after NPs-Hydrogel Treatment

To mimic the OA phenotype *in vitro*, we used a well-established model where chondrocytes are stimulated with a purified 42 kDa endotoxin-free recombinant fibronectin fragment (FN-f) at 1 μM in PBS, prepared as previously described.[48,49] The FN-f consists of domains 7−10 in native fibronectin, which contains the RGD cell-binding domain recognized by the α5β1 integrin. Cells were cultured in Corning 12 transwell plates at 750 k cells/well in DMEM/F-12 with 10% FBS. Two hours before treatment with either FN-f or PBS for control, cells were incubated in a serum-free DMEM/F-12 and then treated for 4 h with FN-f or PBS treatment. Then, cells were washed with PBS and treated for an additional 24 h and 48 h with either 50 μM free DEX in DMEM/F-12 (with 0.1% v/v DMSO, serum-free), DEX-loaded PCL-P(PEGMA) NPs encapsulated in AC-HA hydrogel, or PCL-PDMAEMA NPs encapsulated in AC-HA hydrogel previously placed in a transwell (0.4 μm polyester membrane). After the treatment, the medium was collected and frozen at −80 °C. The medium was used for quantification of inflammatory factors secreted by the cells (IL-6 and TNF-α) through the respective ELISA kit (IL-6: KHC0061, Invitrogen, TNF-α: BMS223-4, Invitrogen). The analysis was conducted on samples treated with FN-f in DMEM/F-12 medium alone (CTRL +), DMEM/F-12 medium alone (CTRL −), DEX-loaded NPs-hydrogels, or free DEX alone.

Cell Morphometric Assessment of Human Chondrocytes after NPs-Hydrogel Treatment

Cells were cultured in Corning 12 transwell plates at 750k cells/well in DMEM/F-12 with 10% FBS. Two hours before treatment, cells were washed with PBS and incubated in a serum-free DMEM/F-12. Then, cells were treated for 48 h with either PBS (untreated control), pristine AC-HA hydrogels, AC-HA hydrogels with DEX-loaded PCL-P(PEGMA) NPs, or AC-HA hydrogels with DEX-loaded PCL-PDMAEMA NPs, previously placed in the transwell basket (0.4 μm polyester membrane). After the treatment, the media was removed, and cells were thoroughly washed with PBS. Cells were successively treated with 1 μM CalceinAM solution and incubated for 30 min for staining. Cells were observed using an EVOS M5000 microscope equipped with an EVOS Olympus 20× objective (AMEP4906). The images were acquired with the GFP (green) channel ($\lambda_{ex}/\lambda_{em}$ = 470/525 nm) and processed with ImageJ to study cell morphology.

Statistical Analysis

Analysis of variance (ANOVA) was used to analyze the experimental data obtained with Tukey post-hoc tests for comparison of different groups and evaluation of the p-value. Statistical significance was set at the top value of <0.05. Results were presented as mean value ± standard deviation, $*p < 0.05$; $**p < 0.01$; $***p < 0.001$, and $****p < 0.0001$.

3. RESULTS AND DISCUSSION

3.1. Polymer Design and Characterization

To develop a series of composite systems based on a hydrogel matrix incorporating polymeric NPs, three amphiphilic copolymers were synthesized by varying the hydrophilic segment to finely tune the physicochemical properties of the resulting assemblies.

The block copolymers were prepared via a sequential combination of ROP and ATRP, where the hydrophobic block consisted of PCL, while the hydrophilic segments were composed of P(PEGMA), PGMA, or PDMAEMA, selected to impart specific functionalities.

PCL-P(PEGMA) copolymer was selected due to the inert nature of the P(PEGMA) corona with respect to the hydrogel matrix. As a result, its encapsulation within the AC-HA system

https://doi.org/10.1021/acsbiomaterials.6c00470
ACS Biomater. Sci. Eng. XXXX, XXX, XXX−XXX

is exclusively governed by the physical entrapment of the NPs within the cross-linked gel network. By contrast, PCL-PGMA copolymer contains PGMA side chains, each bearing two free hydroxyl groups (−OH) per repeating unit, which can form covalent bonds with the hydrogel matrix. These reactive groups can actively participate in the polycondensation reaction employed to obtain gelation, thereby facilitating chemical integration of the NPs into the hydrogel network. Lastly, PCL-PDMAEMA copolymer carries positive charges at physiological pH, arising from the protonation of the terminal tertiary amine groups present in the DMAEMA segments. In this case, electrostatic interactions can occur between the positively charged copolymer and the negatively charged hydrogel matrix, further influencing the incorporation and stability of the NPs within the gel.

PCL_n blocks were synthesized by bulk ROP of ε-caprolactone using BnOH as initiator and $Sn(Oct)_2$ as catalyst. High monomer conversion ($\chi_{ROP} > 98\%$) was achieved, as determined by ^{1}H NMR spectroscopy, yielding polymers with defined DP and molecular weight. The terminal hydroxyl groups of PCL_n chains were quantitatively converted to isobutyryl bromide end-groups, generating PCL_n-Br macroinitiators suitable for the subsequent ATRP of the hydrophilic blocks as previously reported.[17,18]

PCL_n-$P(PEGMA)_m$ copolymers were obtained via ATRP of PEGMA macromonomer, using Cu(I)Br/HMTETA catalytic system in THF.[17] Analogously, PCL_n-$PDMAEMA_m$ copolymers were synthesized by ATRP of DMAEMA in MeOH, catalyzed by Cu(I)Br/BPY complex. On the other hand, PCL_n-$PGMA_m$ macromolecule was produced through an activator regenerated by electron transfer (AGET) ATRP of GMA, utilizing $CuCl_2$/TPMA, with ascorbic acid as the reducing agent in DMF, to ensure more controlled polymerization behavior.[17,50] The detailed synthesis pathways followed are reported in Figure S5 (Supporting Information).

The amphiphilic copolymers were engineered to self-assemble into structures exhibiting a core-shell architecture. For all copolymers, the PCL_n block length was set to 30 units ($n = 30$); likewise, the hydrophilic block was designed with 30 repeating units ($m = 30$). This architecture enabled the formation of NPs with a sufficiently large hydrophobic domain to accommodate lipophilic compounds, while maintaining stability in aqueous media.[17,20,51] ATRP of PEGMA, DMAEMA, and GMA consistently yielded high monomer conversions ($\chi_{ATRP} \geq 90\%$ after 6 h by ^{1}H NMR) while SEC analysis corroborated these findings with narrow M_n distributions ($Đ < 1.3$) and the target lengths. A detailed summary of the copolymer compositions and their characterization is provided in Table 1. The observed discrepancies between M_n values determined by ^{1}H NMR and SEC are attributed to the inherent limitations of SEC, particularly those associated with calibration against polystyrene standards, as previously reported.[17−19]

A representation of the copolymer structure is shown in Figure 2. ^{1}H HNMR spectra of the purified polymers are presented in the Supporting Information (Figure S6), along with corresponding SEC chromatograms (Figure S7).

3.2. Nanoparticle Formulation, Drug Loading, and Release

NPs derived from the synthesized macromolecules were prepared using a nanoprecipitation technique followed by solvent evaporation, as previously described.[17,18] The nanoassemblies were dispersed either in 10 mM PBS at pH 7.4 or in Milli-Q water, and subsequently characterized by DLS at 25 °C.

Table 1. Summary of Design Parameters and Characterization Data of PCL_n-$P(PEGMA)_m$, PCL_n-$PGMA_m$, and PCL_n-$PDMAEMA_m$ Copolymers[a]

polymer	n [-]	m [-]	$M_{n,\,NMR}$ [kDa]	$M_{n,\,SEC}$ [kDa]	Đ [-]
PCL_n-$P(PEGMA)_m$	30	27	17.1	20.4	1.1
PCL_n-$PGMA_m$	29	29	8.1	9.6	1.2
PCL_n-$PDMAEMA_m$	30	30	8.7	10.4	1.1

[a] $M_{n,NMR}$ and $M_{n,SEC}$ represent the number-average molecular weight obtained by ^{1}H NMR and SEC, respectively, where Đ is the dispersity (by SEC). n and m correspond to the degree of polymerization of the hydrophobic and hydrophilic blocks of the polymers, respectively.

The list of formulated NPs, along with their Z-average sizes, PdI, and ζ-potential values, is provided in Table 2. The corresponding size distribution curves and average ζ-potential are presented in Figure 3 (ζ-potential distribution curves are reported in Figure S8, Supporting Information).

All NPs exhibited monomodal size distribution profiles, with a single peak accounting for 100% of the scattering intensity and PdI values below 0.2, indicating narrow size distributions and high sample uniformity. Regardless of the hydrophilic monomer employed, all micelles displayed an average hydrodynamic diameter (D_h) between 45 and 50 nm. Consequently, they are expected to have the same steric hindrance when incorporated into hydrogel matrices.

The most notable difference among the formulations was observed in the ζ-potential measurements. As anticipated, PCL-P(PEGMA) and PCL-PGMA-based particles were approximately neutral; in contrast, PCL-PDMAEMA micelles exhibited a markedly positive surface charge with a ζ-potential of approximately +30 mV. This is ascribed to the partial protonation of the DMAEMA units under physiological pH conditions.

NPs were loaded with a synthetic hydrophobic drug in order to assess their encapsulation efficiency and drug loading performance. For this purpose, DEX was selected, given its widespread use in the treatment of inflammatory conditions.[37−39,52,53] DEX was encapsulated by co-dissolving it with the polymer in acetone prior to nanoprecipitation.

The drug-to-polymer mass ratio was fixed at 1:10 (w/w) across all formulations to remain below the maximum drug loading capacity of this class of polymeric systems.[17,20] The polymer concentration was maintained at 20 mg/mL, based on previous studies indicating that the highest drug loading efficiencies are achieved at moderate polymer and drug concentrations (20 mg/mL polymer and 10% drug, w/w).[19,20,54]

Table 2 summarizes the DL (%) and EE (%) values obtained via HPLC analysis for DEX-loaded NPs, formulated with the three different copolymers. As expected, the data show very similar physicochemical characteristics across the formulations, with an average EE of 35% and a DL of 3.3%, given that the hydrophobic cores of all three NP types were composed of PCL having identical molecular weights.

Finally, DEX release from the NPs was investigated over a period of 5 days to evaluate the rate and extent of drug release in aqueous buffer under sink conditions, at 37 °C and pH 7.4. Drug release kinetics were monitored by HPLC, and the resulting profiles are presented in Figure S9 (Supporting Information).

https://doi.org/10.1021/acsbiomaterials.6c00470
ACS Biomater. Sci. Eng. XXXX, XXX, XXX−XXX

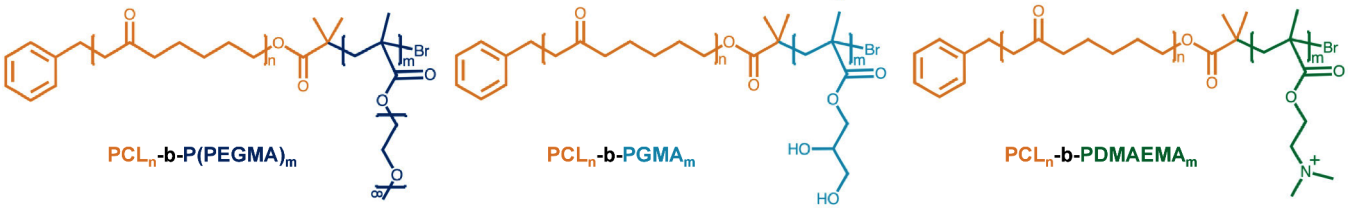

Figure 2. Chemical structure of PCL$_n$-P(PEGMA)$_m$, PCL$_n$-PGMA$_m$ and PCL$_n$-PDMAEMA$_m$ block copolymers.

Table 2. Summary of Physicochemical Properties and Drug Encapsulation Performances of PCL-P(PEGMA), PCL-PGMA, and PCL-PDMAEMA NP Suspensions Recorded via DLS and HPLC Analysis[a]

polymer	Z-Av. Size [nm]	ζ-pot. [mV]	PdI [-]	EE [%]	DL [%]
PCL-P(PEGMA)	45 ± 1	1.2 ± 0.8	0.14	32.4 ± 0.9	3.1 ± 0.7
PCL-PGMA	47 ± 2	−1.3 ± 0.8	0.15	33.7 ± 1.2	3.2 ± 0.4
PCL-PDMAEMA	50 ± 2	30.2 ± 1.5	0.18	36.8 ± 1.4	3.7 ± 0.6

[a]Reported values represent the mean ± standard deviation, calculated from a minimum of three replicates per sample.

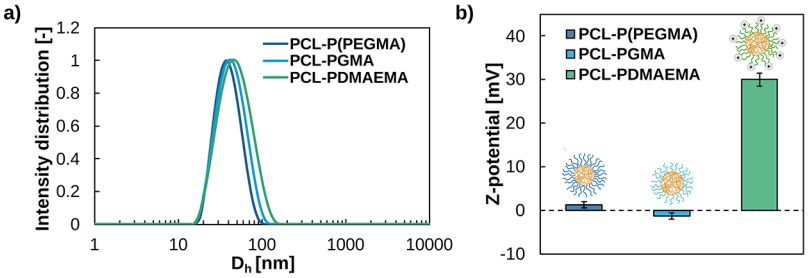

Figure 3. (a) DLS size distribution curves of the three NP formulations in water at 25 °C (1 mg/mL) and (b) average ζ-potential of PCL-P(PEGMA), PCL-PGMA and PCL-PDMAEMA NPs in water at 25 °C (0.3 mg/mL).

No significant differences were observed in the release behavior among the different polymeric formulations, with all release curves reaching a plateau close to 100% within approximately 24 h. Given that polymer degradation was negligible over the timescale of the experiment,[20] the DEX release mechanism was primarily attributed to passive diffusion.

Additionally, the presence of DEX did not induce notable changes in particle size as previously observed.[17] Therefore, it is reasonable to conclude that drug diffusion was governed predominantly by the surface area of the colloids, and hence by the particle size, which was almost the same across all formulations. The experimental data obtained were fitted with the Korsmeyer-Peppas (KP) and Peppas-Sahlin (PS) models (eqs 3 and 4, respectively) to confirm the mechanism involved in the DEX release from the NPs. Both models are empirical or semi-empirical approaches commonly employed to characterize drug release kinetics from polymeric matrices. The PS model is an extension of the KP equation, allowing the mathematical distinction of Fickian diffusion and polymer relaxation/swelling effects. In Table S1 (Supporting Information) are reported the coefficients describing the two models obtained from the mathematical fitting and the corresponding R^2 values.

These outcomes indicated a diffusion-dominated release, as expected for nanometrically sized delivery systems. Moreover, the release exponent n was consistently close to 0.43 for all three particle types, confirming that the release followed a Fickian diffusion model.

3.3. NPs-Hydrogel Composite Systems Formulation: Chemical, Ionic, and Physical NP Loading

The formulated NPs have been successively employed as building blocks for the assembly of the NPs-hydrogel composites. The hydrogel consisted of agarose, carbomer, and HA formulation, where the latter represents the most abundant component of the polymer mixture (composition details are shown in Figure 4a).[55] HA was employed as a partial substituent for carbomer from a formerly optimized hydrogel formulation (agarose-carbomer, AC).[24,25] HA is a naturally derived, biodegradable, and biocompatible polymer widely employed in biomedical applications, being part of some biological fluids.[56,57] In particular, it is present in synovial fluid and cartilage extracellular matrix, where it contributes to lubrication, viscoelastic damping, and joint homeostasis. Its high water-binding capacity and polyanionic nature enable the formation of highly hydrated networks that support diffusion-based drug delivery while preserving tissue compatibility and reducing cytotoxicity.[58] HA is advantageous over other natural or synthetic polymers, e.g., alginate or gelatin, as the latter usually need ionic cross-linking and are characterized by poor NP retention, dispersion, and controlled release.[59] In this regard, HA modulates the swelling behavior, which can influence the release kinetics of the encapsulated payload by affecting diffusion pathways within the network. In addition, HA free carboxyl groups are essential for the selected gelation mechanism, while its molecular weight can be tuned to modulate mesh size and

https://doi.org/10.1021/acsbiomaterials.6c00470
ACS Biomater. Sci. Eng. XXXX, XXX, XXX−XXX

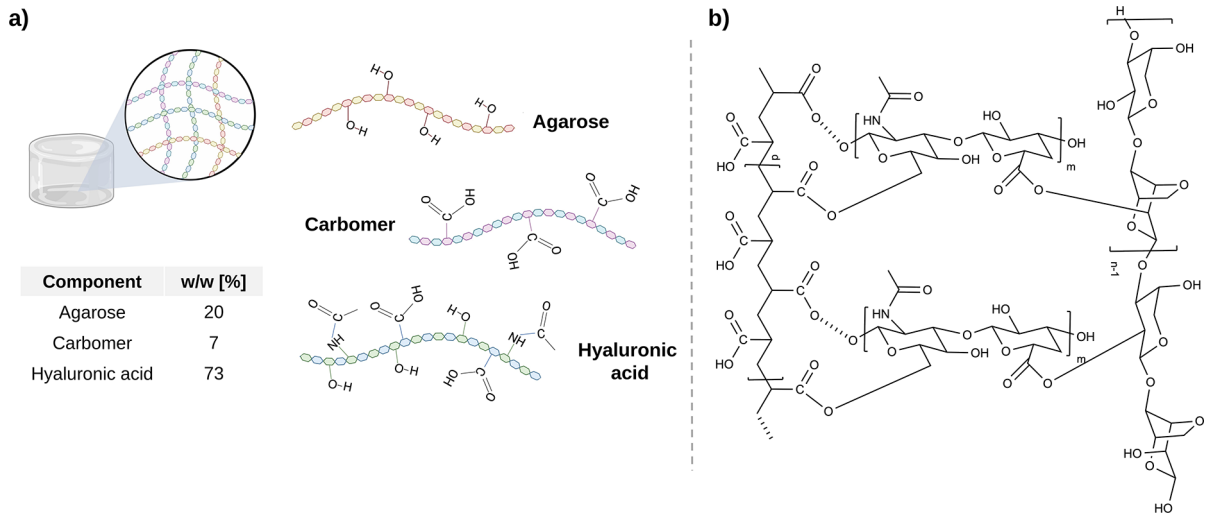

Component	w/w [%]
Agarose	20
Carbomer	7
Hyaluronic acid	73

Figure 4. (a) Sketch of the formulated AC-HA hydrogels, schematic representation of its constituents and w/w % relative composition. (b) Chemical structure of the AC-HA cross-linked network.

degradation rate.[43] Overall, HA combines intrinsic bioactivity and translational relevance, making it a particularly suitable components in anti-inflammatory composite system for osteoarthritis treatment.

Hydrogels based solely on HA are lacking from mechanical properties, however its combination with other polymeric constituents led to hydrogels with improved mechanical properties.[33]

In this context, carbomer was selected due to its high density of carboxylic acid groups, which facilitate efficient esterification reactions and promote robust cross-link formation.[43] Furthermore, it is widely used in pharmaceutical and biomedical formulations as a rheology modifier and gel-forming agent, offering reproducible mechanical properties and scalability. The combination of carbomer with HA allowed for the balance of structural integrity with biological relevance, resulting in a mechanically stable yet biocompatible hydrogel matrix.[60] Similarly, agarose was selected due to its well-established properties as a natural polysaccharide, ensuring excellent biocompatibility, gradual biodegradability, and thermoresponsive gelation behavior. Indeed, agarose solutions undergo thermally induced gelation, forming a stable three-dimensional network when the temperature decreases from the sol state to values close to physiological conditions (~37 °C).[61] Furthermore, previous studies investigating hydrogels based on HA conjugated with various polysaccharides for cartilage repair applications have demonstrated that agarose incorporation can significantly promote tissue restoration. In particular, these systems have been reported to support cartilage regeneration by modulating inflammatory responses and stimulating the expression of genes associated with cartilage formation and autophagy.[62]

The hydrogel was obtained through a microwave-assisted polycondensation reaction occurring between the carboxylic groups (–COOH) of carbomer and hyaluronic acid and the hydroxyl groups (–OH) present in agarose and hyaluronic acid. Microwave irradiation ensures rapid and homogeneous heating of the reaction mixture, promoting efficient esterification between the functional groups of the polymeric components at 80 °C. This reaction leads to the formation of covalent ester bonds, which act as cross-linking points within the resulting three-dimensional polymeric network (Figure 4b). The adopted strategy also allows the facile incorporation of bioactive molecules or colloidal systems, such as NP dispersions, within the matrix prior to the completion of the gelation process, enabling their homogeneous encapsulation inside the hydrogel structure.

The FT-IR spectrum of the hydrogel matrix is reported in Figure S10 (Supporting Information) confirming the occurrence of the polycondensation reaction. A broad absorption band in the 3600−3100 cm^{-1} region corresponds to the stretching vibrations of hydroxyl groups (–OH), including both free hydroxyls and those involved in intra- and intermolecular hydrogen bonding. The region between 3000 and 2750 cm^{-1} is associated with the stretching vibrations of aliphatic C–H bonds in the polymer backbone. A characteristic band observed at 1750−1720 cm^{-1} is attributed to the C═O stretching vibration of ester groups, providing evidence of ester bond formation during the polycondensation process. Additionally, the band in the 1650−1500 cm^{-1} region can be assigned to N−H bending and stretching vibrations of amide groups, originating from the HA structure.

Further contributions are observed in the 1440−1390 cm^{-1} range, which are associated with in-plane C–O–H bending vibrations and C–O stretching. Finally, the broad region between 1400 and 900 cm^{-1} comprises several overlapping signals related to alcohol and ether functionalities, including O–H bending vibrations (1410−1230 cm^{-1}), C–O stretching of ether groups (1400−1200 cm^{-1}), and C–O stretching of alcohol groups (1200-900 cm^{-1}). The presence of ester-related signals together with the reduced contribution of free carboxylic groups indicates that HA actively participates in the esterification reaction, contributing to the formation of the cross-linked matrix. Additional IR spectra, together with further structural characterization of similar agarose-carbomer hydrogels, have been previously reported in the literature.[43,63] These studies consistently corroborate the formation of ester bonds within the polymeric network, accompanied by a parallel attenuation of the absorption bands associated with the carbomer carboxylic (–COOH) groups, supporting the successful esterification and cross-linking.

As illustrated in Figure 5, the formulation procedures used to prepare the various NPs-hydrogel composites differ according to the specific interactions targeted between the functional NPs and the hydrogel network.

https://doi.org/10.1021/acsbiomaterials.6c00470
ACS Biomater. Sci. Eng. XXXX, XXX, XXX−XXX

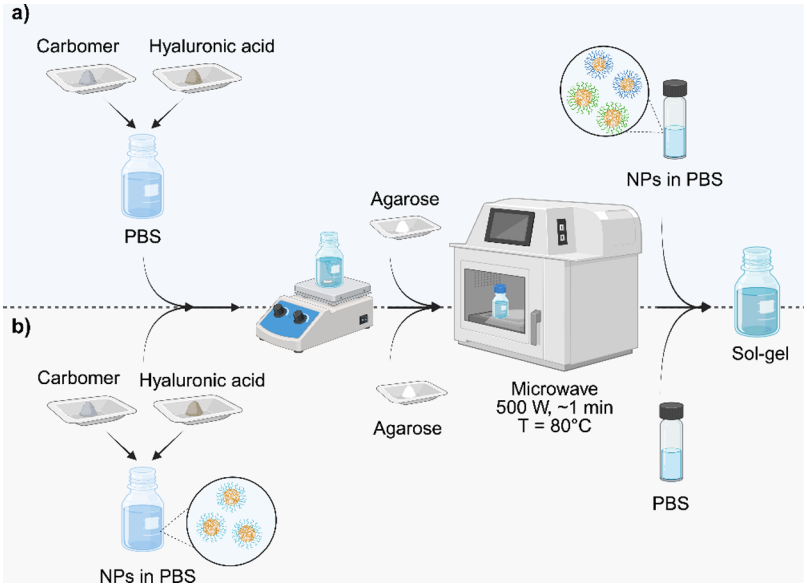

Figure 5. Schematic representation of the formulation processes used for NPs-hydrogel composites: (a) physical or electrostatic encapsulation of inert PCL-P(PEGMA) or cationic PCL-PDMAEMA NPs, respectively, (b) covalent linkage of PCL-PGMA NPs undergoing polycondensation reaction with hydrogel constituents.

Specifically, one method consisted of the physical or ionic entrapment of the NPs in the hydrogel network (Figure 5a), while the second involved the chemical linkage of the NPs to the hydrogel matrix (Figure 5b). In this context, only PCL-PGMA NPs can be subjected to covalent bonding through their terminal −OH groups. On the other hand, PCL-PDMAEMA NPs can assemble with the hydrogel matrix by ionic interaction, given their positively charged surface under physiological conditions, while PCL-P(PEGMA) NPs can be embedded into the system only through physical encapsulation. In the case of covalent encapsulation, the hydrogel constituents were pre-dissolved in the NP solution in PBS, and then subjected to condensation reaction through microwave irradiation; in the case of physical and ionic encapsulation, the NP solution was added to the hydrogel polymers solution (1:1 v/v dilution) before the sol-gel transition.

To validate the feasibility of the chemical encapsulation method, the NP solution alone was subjected to microwave irradiation up to 80 °C.[24,25] NP integrity was assessed through DLS analysis (same conditions previously reported from NP characterization), which did not reveal any evident heat-induced degradation or aggregation phenomena, compared to the freshly prepared NPs, as shown in Figure S11 (Supporting information).

3.4. NPs-Hydrogel Composites Rheological Analysis

Rheological studies were performed on the three formulations to assess the effect of the NPs-hydrogel interactions on the mechanical properties of the system. Amplitude sweep tests demonstrated that all the NPs-hydrogel composites are characterized by a solid-like behavior (with $G' \gg G''$), within the linear viscoelastic (LVE) region, as shown in Figure 6. The hydrogel containing PCL-PDMAEMA NPs showed the highest average

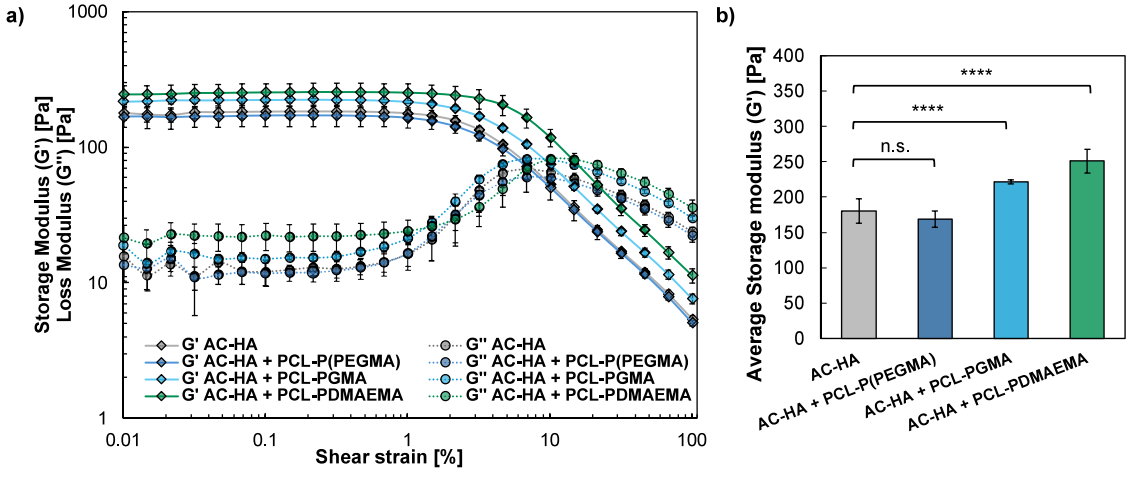

Figure 6. (a) Average G' and G'' from amplitude sweep tests performed on pristine hydrogel and on the three NPs-hydrogel composites (at shear strain values ranging from 0.1% to 100%). Results are presented as mean ± SD ($N = 3$). (b) Average G' values of pristine AC-HA hydrogel and of the three composite system measured within the constant LVE region (0.01%–1% shear strain) (****, $p < 0.0001$).

https://doi.org/10.1021/acsbiomaterials.6c00470
ACS Biomater. Sci. Eng. XXXX, XXX, XXX−XXX

G' value (250 ± 15 Pa), which could be attributed to the electrostatic interaction established within the hydrogel and the cationic NPs, forming additional cross-links between the polymer chains. In contrast, the composite containing PCL-P(PEGMA) NPs showed a G' value closer to the pristine hydrogel (180 ± 8 Pa), due to the lack of significant additional intermolecular interactions. A different behavior was observed with the covalently linked PCL-PGMA NPs, exhibiting a slightly lower G' value compared to PCL-PDMAEMA. While the positive charges of PDMAEMA might all be involved in electrostatic interactions with the surrounding chains, in the case of PGMA, only the −OH groups effectively linked to distinct hydrogel chains would contribute to increasing the cross-linking points. Therefore, while the formation of cross-linking can enhance hydrogel stiffness, this effect is proportional to the number of NPs actively participating in the formation of multiple covalent bonds.

Additionally, the test revealed a slightly more extended LVE region in the case of PCL-PDMAEMA NPs-hydrogel compared to the other cases. This extension is typically associated with an enhanced liquid-like response and with an augmented elasticity of the composite gel, arising from the non-covalent electrostatic interactions established between the components.[64] This was supported by analyzing the value of the $\tan(\delta) = G''/G'$, which increased in the case of encapsulated ionic NPs, showcasing a higher contribution of the viscous modulus G'' on the composite hydrogel final properties, compared to the other two cases (Figure S12, Supporting Information). Frequency sweep tests revealed that the pristine hydrogel maintained its solid-like behavior within a frequency range from 0.1 to 100 rad/s, as shown in Figure S13 (Supporting information).

The average mesh size (ξ) of the hydrogel network was estimated using classical rubber elasticity theory based on the experimentally measured storage modulus in the plateau region of the frequency sweep test ($G' \approx 155$ Pa, Figure S13). According to the relation $\xi = (kT/G')^{1/3}$, where k is the Boltzmann constant (1.38×10^{-23} J K^{-1}) and T is the absolute temperature, the calculated mesh size was approximately 30 nm. In parallel, the corresponding cross-linking density (ν_e) was evaluated as $\nu_e = RTG'$ ($R = 8.314$ J·mol^{-1}·K^{-1}), resulting in 0.062 mol/m^3.

Representative SEM micrographs of the pristine hydrogel and of the NP-loaded hydrogel are reported in the Supporting Information (Figure S14), showing the porous morphology of the lyophilized polymeric network. The micrographs revealed a highly porous and interconnected network in all samples, with no significant differences in pore morphology upon NP incorporation, indicating that the presence of NPs does not alter the internal hydrogel architecture. Direct visualization of the NPs is inherently challenging due to their low concentration and nanoscale dimensions (45−50 nm), in combination with their soft polymeric nature, which results in a chemical composition and electron density closely matching that of the surrounding hydrogel matrix. Nevertheless, visual inspection of the NPs-hydrogels, prepared with fluorescently labeled NPs (Figure S15, Supporting Information) revealed homogeneous color distribution without evidence of NP precipitation or aggregation. Although nanoscale rearrangements cannot be excluded based on visual inspection alone, no macroscopic instability or phase separation was observed.

3.5. Effect of the Encapsulation Method on NP Release

Successively, the NPs-hydrogel composites were immersed in PBS at 37°C to evaluate the release or retention of the NPs from the matrix, according to the NPs-hydrogel interactions. In order to assess NP release profiles, PCL-PGMA and PCL-P(PEGMA) NPs were both subjected to chemical and physical encapsulation schemes (Figure 5a,b, respectively) at a fixed concentration.

As expected, PCL-P(PEGMA) NPs exhibited a nearly identical release profile regardless of the encapsulation method, with closely 100% of the NPs released after ∼3 days, as shown in Figure 7a (PCL-P(PEGMA) encaps. and PCL-P(PEGMA) chemical). This behavior confirms the inability of PCL-P(PEGMA) NPs to bind any hydrogel constituents, due to the chemical inertness of P(PEGMA). On the other hand, PCL-PGMA NPs showed a different release behavior depending on the encapsulation method. When chemical linkage was achieved, NPs were partially retained inside the hydrogel matrix, with only around 33% of the NPs being released over 5 days (Figure 7a, PCL-PGMA chemical, and Figure 7b). By contrast, in the case of physical encapsulation, the above-mentioned NPs followed the same release profile showcased by the PCL-P(PEGMA) ones (Figure 7a, PCL-PGMA encaps.).

A comparable release study was conducted using the PCL-PDMAEMA NPs to assess the influence of the NPs-hydrogel electrostatic interactions on NP retention. Similar to the chemically linked PCL-PGMA NPs, the cationic NPs were strongly retained within the hydrogel network. As shown by the release profile, only approximately 22% of PCL-PDMAEMA NPs were released within the first 24 h, underscoring the hydrogel's ability to function as a reservoir for both positively charged and covalently bound NPs (Figure 7b).

Also in this case, the release curves were fitted to assess the mechanism involved in NP release from the composite hydrogels. The obtained coefficients are reported in Table S2 (Supporting Information), with the corresponding R^2 values.

For all formulations, the resulting equations can be recast into the KP model. For PCL-P(PEGMA) and PCL-PDMAEMA NPs, the release exponent $n = 0.40$−0.45 indicates a Fickian or quasi-Fickian diffusion process. In contrast, for PCL-PGMA NPs, the exponent $n = 0.76$ suggests an anomalous transport mechanism, given by the additional chemical interactions with the hydrogel constituents. The experiments were repeated under mild acidic conditions (pH 5) at 37 °C to investigate the pH influence on the NP release behavior. The selected conditions may mimic the microenvironment of inflamed or diseased tissues, representing a relevant context for the possible application of this drug delivery platform.

The release profiles, displayed in Figure 7c, show that both PCL-PDMAEMA and PCL-P(PEGMA) NPs tend to be more retained by the hydrogel when in an acidic environment. This behavior could be ascribed to the tighter hydrogel matrix, resulting from the reduced repulsion between the hydrogel polymeric chains, thanks to charge shielding exerted by the H^+ ions at lower pH. In this case, the swelling is reduced and consequently the average pore size, thus inhibiting NP release. However, the difference is more significant for PCL-PDMAEMA NPs. At pH 5, the latter were almost completely retained from the hydrogel network, showing just 5% release within 5 days. In this case, despite the simultaneous hydrogel chain protonation, the PCL-PDAMEMA NP ξ-potential increase (47 ± 2 mV rather than 32 ± 1 mV under physiological conditions, Figure S8b, Supporting Information) offers a more relevant contribution in enhancing NPs-hydrogel interaction and thus NP retention.

https://doi.org/10.1021/acsbiomaterials.6c00470
ACS Biomater. Sci. Eng. XXXX, XXX, XXX−XXX

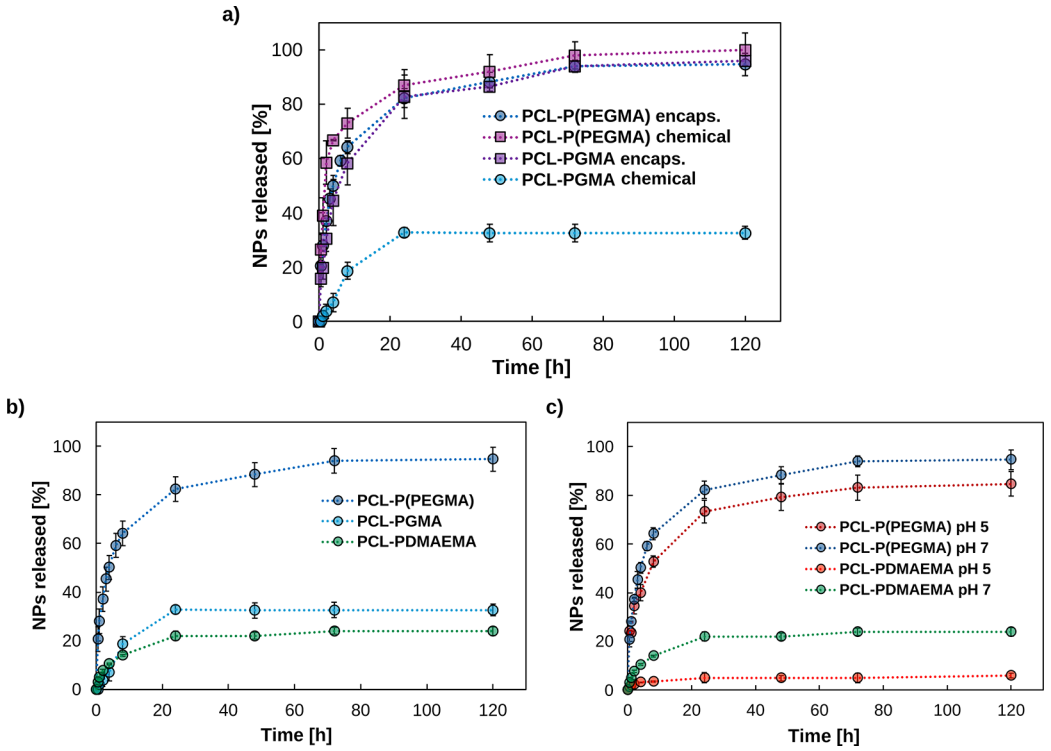

Figure 7. (a) Comparison of the cumulated NP release from the NPs-hydrogel composite systems using either the physical or the chemical encapsulation method for PCL-P(PEGMA) and PCL-PGMA NPs in PBS at 37 °C under sink conditions. (b) Cumulated NP release from the NPs-hydrogel composites containing the physically encapsulated PCL-P(PEGMA) NPs, chemically encapsulated PCL-PGMA NPs, or ionically encapsulated PCL-PDMAEMA NPs in PBS pH 7.4 at 37 °C under sink conditions. (c) Comparison of the cumulated NP release from the NPs-hydrogel composite systems containing PCL-P(PEGMA) NPs and PCL-PDMAEMA NPs at physiological (pH 7.4) and slightly acidic (pH 5) conditions, at 37 °C (under sink conditions).

3.6. Drug Release from the Composite Systems

Following the characterization of the hydrogel's capability to retain or release the NPs, drug release studies were conducted for the three systems to evaluate the influence of NPs-hydrogel physicochemical interactions on therapeutic release kinetics. In this perspective, two scenarios were investigated: a hydrophobic drug (DEX) encapsulated in the NPs, and a hydrophilic molecule (BSA) co-encapsulated in the hydrogel matrix with the NPs. The NPs-hydrogel composites were formulated as previously described, employing DEX-loaded NPs for this purpose.

Concerning DEX release, the experiments were conducted in aqueous buffer at 37 °C and pH 7.4, under sink conditions, and the extent of drug released over time was quantified via HPLC.

The drug release curves, presented in Figure 8a, demonstrate that the NPs-hydrogel interaction mechanism is able to significantly slow down the rate of DEX diffusion from the system, compared to the case of free NPs (Section 3.1, Figure S9). While DEX was completely released from the free NPs within approximately 24 h, sustained release was observed until 6−14 days from the NPs-hydrogel composites. More specifically, in the case of PCL-P(PEGMA), DEX was gradually released until 100% after 6 days. This behavior can be attributed to the concurrent diffusion of the NPs out of the hydrogel matrix. In contrast, for PCL-PGMA and PCL-PDMAEMA loaded gels, DEX release was markedly slower, approaching a maximum of 86% and 62%, respectively, within 14 days. This outcome is likely due to the effective retention of the majority of NPs within the hydrogel network (as discussed in Section 3.4), requiring the drug to first diffuse out of the NPs and subsequently through the hydrogel, thereby leading to a more sustained overall release. The parameters describing the DEX release model are reported in Table S3 (Supporting Information). The release equations derived for the three systems can be reduced to the KP model with quasi-Fickian or Fickian behavior ($n = 0.41-0.45$).

The therapeutic release ability of the NPs-hydrogel composite was additionally investigated with the encapsulation of a BSA-FITC within the hydrogel matrix. BSA was selected as a drug mimetic for the test, owing to the well-characterized features, such as size, electrostatic profile at physiological pH, and diffusion behavior. BSA, with its hydrodynamic diameter of ∼7 nm, closely resembles properties of different protein-based drugs, such as enzymes, cytokines, fusion proteins, or monoclonal antibodies (mAb),[23,65] employed for various therapeutic applications. The NPs-hydrogel composites were formulated, encapsulating BSA-FITC according to the above-mentioned procedure. The release tests were performed in an aqueous buffer, at 37 °C and pH 7.4, and the amount of protein released was characterized via UV-vis spectroscopy.

The cumulated BSA release profiles, presented in Figure 8b, showed different behaviors in terms of kinetics and plateau values, depending on the NPs employed in the formulation. In the case of PCL-PDMAEMA NPs, the protein diffusion rate was consistently lower and limited compared to that of the other cases. More in detail, for PCL-P(PEGMA) and

https://doi.org/10.1021/acsbiomaterials.6c00470
ACS Biomater. Sci. Eng. XXXX, XXX, XXX−XXX

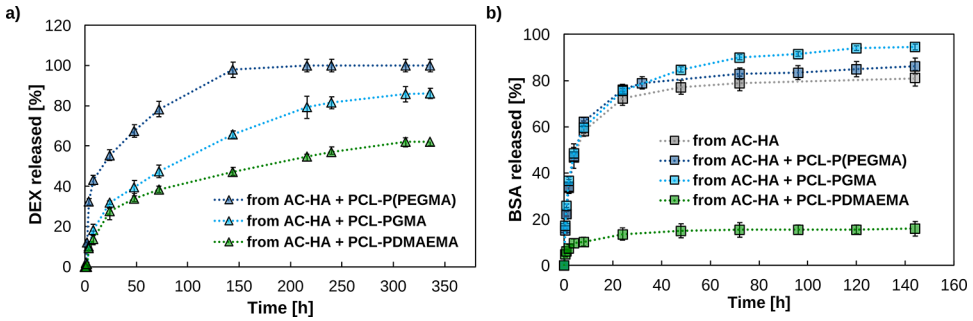

Figure 8. (a) Cumulated DEX release (in PBS at 37 °C under sink conditions) from the NPs-hydrogel composite systems containing either the physically encapsulated PCL-P(PEGMA) NPs, chemically encapsulated PCL-PGMA NPs or ionically encapsulated PCL-PDMAEMA NPs. (b) Cumulated BSA release (in PBS at 37 °C under sink conditions) from composite hydrogels with either physically encapsulated PCL-P(PEGMA) NPs, chemically encapsulated PCL-PGMA NPs, ionically encapsulated PCL-PDMAEMA NPs, or without NPs.

PCL-PGMA NP-loaded systems, 86% and 94% of BSA-FITC, respectively, were released in 6 days. On the other hand, the systems formulated with PCL-PDMAEMA NPs showed a plateau at 15% release after 24 h. The observed behavior was likely due to the electrostatic interactions between the negatively charged BSA (isoelectric point at pH 5.1−5.5)[66] and the cationic micelles. Accordingly, almost 85% of the protein was retained inside the NPs-hydrogel system.

For all BSA release systems investigated, regardless of the type of NPs incorporated, the release profiles are well described by the KP model (Table S4, Supporting Information). In both the pristine hydrogel and in the presence of PCL-PEGMA and PCL-PGMA NPs, a Fickian or quasi-Fickian diffusion mechanism is predominant. In contrast, for positively charged PCL-PDMAEMA NPs, the value $n = 0.26$ is consistent with an anomalous mechanism arising from electrostatic interactions between the positively charged particles and the negatively charged protein.

These results clearly demonstrated how the different surface properties of NPs, obtained by simple chemical modifications of the hydrophilic copolymer blocks, are able to modify the release properties of drugs in a composite system.

3.7. Nanoparticles-Hydrogel Composite *In Vitro* Therapeutic Efficacy

The cytotoxicity of NPs-hydrogel composites was investigated before proceeding with successive *in vitro* functional assays. The AC-HA hydrogel is primarily composed of natural polymers, with only a minimal fraction of carbomer. These constituents are widely recognized for their low cytotoxicity. On the other hand, although NPs were synthesized from biocompatible polymers, the potential cytotoxicity of the composites required careful assessment. NPs-hydrogel mixtures were prepared with varying NP concentrations (in the range 1−100 μM) and tested on human-derived chondrocytes to reflect their potential application as a therapeutic platform for OA treatment.

The results, evaluated through LIVE/DEAD assay, are presented in Figure 9a,b (live and dead controls are shown in Figure S16, Supporting Information). The cells treated for 24 h showed a constant viability of around 90%, regardless of the NP type and concentration employed. This demonstrated the low cytotoxic effect of the combined NPs and AC-HA systems. Free DEX, administered at various concentrations, also demonstrated no cytotoxic effects on the cells, further confirming the suitability and applicability of the proposed delivery system.

As proof of the mechanism of the potential anti-inflammatory action of the proposed systems, the secretion of pro-inflammatory cytokines (specifically IL-6 and TNF-α) was assessed on human chondrocytes, after inflammatory state induction and NPs-hydrogel treatment. In this perspective, the FN-f model was used to induce cell inflammation, as reported by previous works (Figure 9c).[67,68]

Considering the outcomes of the results presented in Section 3.5, the anti-inflammatory treatment was performed only using hydrogels loaded with PCL-P(PEGMA) and PCL-PDMAEMA NPs, since the latter showed a closely similar DEX release profile with respect to PCL-PGMA NPs within the first 48 h. The results are represented as a ratio of cytokine release from cells treated with therapeutics and CTRL+. The bar plot reported in Figure 9d,e and Figure S17 shows a significant decrease of both TNF-α and IL-6 secretion when the cells were treated with either free DEX or the DEX-loaded NPs-hydrogel, compared to the untreated control. More specifically, over the considered timeframe, DEX released from the PCL-PDMAEMA system was able to restore cytokine levels to those observed in non-inflamed cells. In contrast, in the PCL-P(PEGMA) formulation, the faster drug release led to enhanced drug accumulation within the volume used for cell treatment in the experiment. This resulted in a more pronounced inhibition of the cytokine expression. Additionally, the effect of PCL-P(PEGMA) was more pronounced than that of free DEX. Indeed, the composite system enables the DEX administration to be sustained over time compared to one-shot free drug administration.

To evaluate whether the hydrogel and drug-loaded nanocomposites influenced chondrocyte morphology, representative fluorescence micrographs of human-derived chondrocytes treated with culture medium and PBS (control), pristine hydrogel, and hydrogels containing DEX-loaded PCL-P(PEGMA) or PCL-PDMAEMA NPs are shown in Figure 10a−d. Cells exhibited comparable morphology across all tested conditions, maintaining the characteristic features of human-derived chondrocytes, which typically display a predominantly rounded shape with minimal spreading under *in vitro* conditions.

To further support this observation, a quantitative morphometric analysis was performed using ImageJ software

https://doi.org/10.1021/acsbiomaterials.6c00470
ACS Biomater. Sci. Eng. XXXX, XXX, XXX−XXX

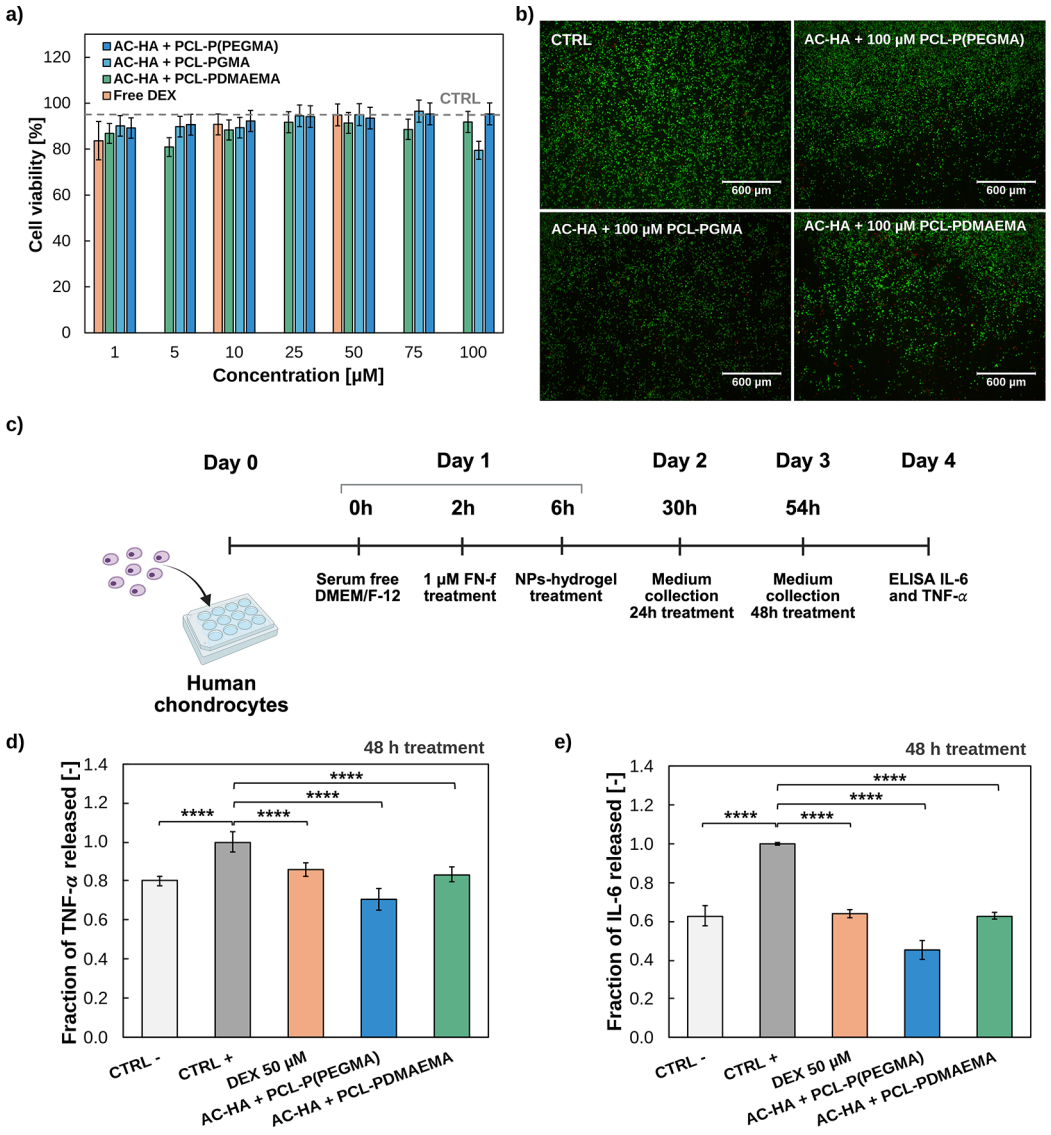

Figure 9. (a) Cell viability from LIVE/DEAD assay performed with different concentrations of free DEX or of PCL-P(PEGMA), PCL-PGMA and PCL-PDMAEMA NPs mixed into AC-HA sol-gel solution (CTRL line refers to cells cultured only with medium). Results are presented as mean ± SD ($N = 4$). (b) Fluorescence microscopy images of the cells treated with only medium or 100 μM PCL-P(PEGMA), PCL-PGMA, and PCL-PDMAEMA NPs mixed with AC-HA solution (green: live cells, red: dead cells). (c) Timeline of FN-f inflammatory activation and subsequent DEX-loaded NPs-hydrogel administration for TNF-α and IL-6 detection. (d) Fraction of TNF-α released after 48 h from treatment with free DEX, or with DEX-loaded NPs-hydrogels composites (CTRL− represents untreated cells while CTRL+ refers to inflamed cells activated by FN-f 7−10 but not treated with therapeutics). (e) Fraction of IL-6 released after 48 h from treatment with free DEX, or with DEX-loaded NPs-hydrogels composites (CTRL- represents untreated cells while CTRL+ refers to inflamed cells activated by FN-f but not treated with therapeutics). Results are presented as mean ± SD ($N = 6$), ****$p < 0.0001$).

(Figure 10e,f). Circularity, roundness, and aspect ratio (AR) were evaluated to assess potential changes in cell shape and elongation. Across all experimental groups, these parameters showed comparable values, and no statistically significant differences were detected ($p > 0.05$) between control, hydrogel-treated, and NPs-hydrogel-treated cells, indicating that neither the pristine hydrogel nor the NP-loaded systems induced detectable changes in cell spreading or elongation.

Circularity values ranged approximately between 0.6 and 0.7, while roundness values were between 0.7 and 0.8, with AR values around 1.2−1.4. These values are consistent with the moderately spread morphology commonly observed for chondrocytes cultured in two-dimensional environments.

Overall, the analysis suggests that the pristine and NPs-loaded hydrogels do not induce detectable alterations in chondrocyte morphology compared with the control conditions.

4. CONCLUSIONS

The combination of hydrogel and NPs represents a promising strategy to design hybrid composite systems as next-generation platforms for drug delivery applications. In this work, three amphiphilic block copolymers were synthesized via controlled/living polymerization techniques, achieving macromolecules with different end-chain functionalities, i.e., inert methyl groups, hydroxyl groups, or ionizable tertiary amines. The polymers were

https://doi.org/10.1021/acsbiomaterials.6c00470
ACS Biomater. Sci. Eng. XXXX, XXX, XXX−XXX

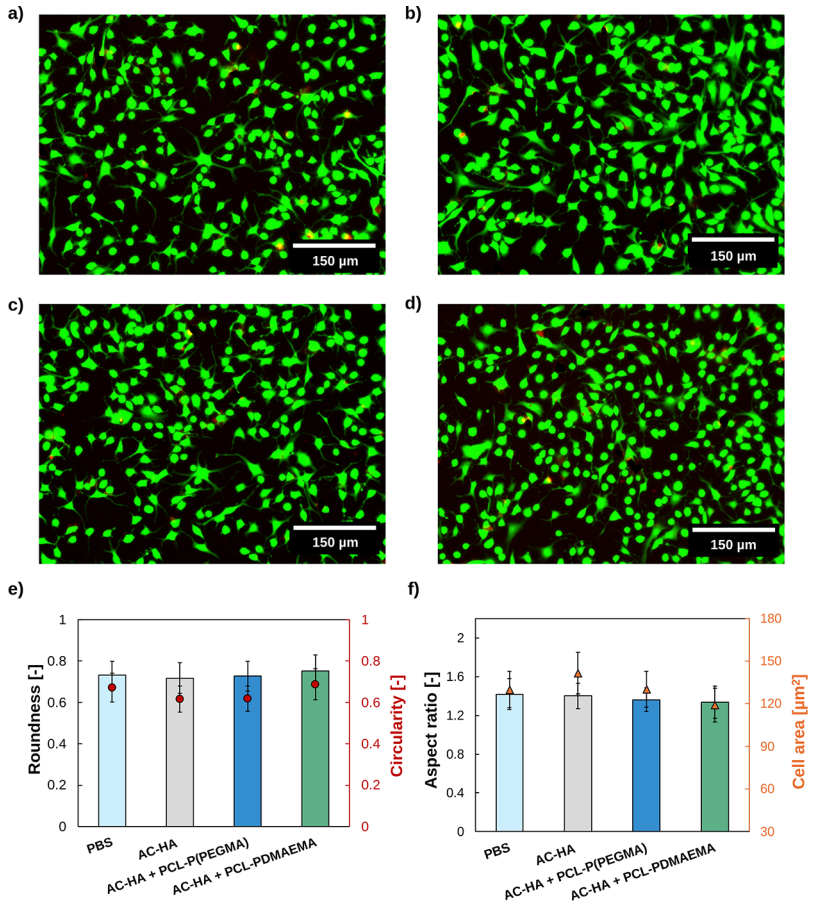

Figure 10. Fluorescence microscopy images of the cells acquired after 48 h of treatment respectively with (a) medium and PBS solution, (b) AC-HA pristine hydrogel, (c) PCL-P(PEGMA) NP-loaded AC-HA hydrogel, and (d) PCL-PDMAEMA NP-loaded AC-HA hydrogel (green: live cells, red: dead cells). (e) Cell roundness (bars) and circularity (circles) average values calculated with ImageJ software for samples treated with culture medium and PBS (control), pristine hydrogel, and hydrogels containing DEX-loaded PCL-P(PEGMA) or PCL-PDMAEMA NPs. Results are presented as mean ± SD (N = 300 cells). (f) Cell AR (bars) and area (triangles) average values calculated with ImageJ software for samples treated with culture medium and PBS (control), pristine hydrogel, and hydrogels containing DEX-loaded PCL-P(PEGMA) or PCL-PDMAEMA NPs. Results are presented as mean ± SD (N = 300 cells).

formulated into core-shell micelles and then included within a cross-linked hydrogel matrix through different encapsulation methods (physical, chemical, or ionic), by harnessing the interplay between the hydrogel and the NP surface moieties.

The inclusion of polymeric NPs inside the hydrogel provided three main advantages: (1) it allowed for encapsulation of a hydrophobic drug, i.e., DEX, inside an otherwise hydrophilic environment; (2) it provided a local confinement of the NPs in a specific space; (3) it prevented the fast diffusion of DEX from the NPs, enhancing the time of drug effectiveness.

Both intermolecular interactions and the encapsulation method demonstrated an influence on NP retention and hydrogel mechanical properties. The system containing chemically and ionically encapsulated NPs showcased a limited NP release, acting as a proper NP reservoir. Additionally, improved mechanical properties were displayed in the chemically or ionically linked NPs, compared to the pristine hydrogel. The composite systems demonstrated tunable DEX release kinetics, with prolonged and sustained release (6−14 days, according to the encapsulation method) compared to the colloidal NPs. Moreover, the platform confirmed the ability to modulate the release of macromolecular hydrophilic cargos (BSA), depending on the NP surface charge, with positively charged micelles exhibiting stronger protein retention within the hydrogel. All formulations showed excellent cytocompatibility with human chondrocytes and effectively reduced pro-inflammatory cytokine expression (IL-6 and TNF-α) in an *in vitro* OA inflammatory model, demonstrating the potential application in OA treatment.

From a translational perspective, the proposed nanocomposite platform leverages fabrication strategies compatible with scale-up and pharmaceutical processing. Nanoprecipitation is a robust and widely adopted technique for polymeric NP production at an industrial scale, allowing precise control over particle size distribution and reproducibility. Similarly, microwave-assisted polycondensation enables rapid and homogeneous hydrogel cross-linking within short reaction times, minimizing thermal gradients, typical of conventional heating, thus supporting batch-to-batch consistency. To ensure sterility and clinical safety, NP suspensions can be sterile-filtered prior to hydrogel incorporation (as performed during *in vitro* tests), while hydrogel components can be processed aseptically, and terminal sterilization methods such as gamma irradiation or ethylene oxide treatment may be applied. While further studies on long-term

https://doi.org/10.1021/acsbiomaterials.6c00470
ACS Biomater. Sci. Eng. XXXX, XXX, XXX−XXX

stability, shelf-life, and large-scale reproducibility are warranted, the modular and chemically defined nature of the system provides a strong foundation for translational development.

Overall, these findings demonstrate that tailoring the NP functionalities solely through polymer chemistry enables the design of multifunctional NPs-hydrogel composites with tunable properties.

The proposed strategy opens new perspectives for future applications, aiming at obtaining tailored drug delivery performances through accurate NPs and macromolecular interaction engineering.

■ ASSOCIATED CONTENT

Supporting Information

The Supporting Information is available free of charge at https://pubs.acs.org/doi/10.1021/acsbiomaterials.6c00470.

Synthesis and purification procedure of: PCL_n and PCL_n-Br; DEX calibration curve recorded via HPCL for quantification of DL, EE and % of release; NP calibration curve based on RhB absorbance at 564 nm via UV−vis analysis; NP calibration curve based on NPs derived count rate measured via DLS; BSA-FITC calibration curve based on FITC absorbance at 495 nm via UV−vis analysis; ATRP reaction scheme for the polymerization of PCL_n-P(PEGMA)$_m$, PCL_n-PGMAm, and PCL_n-PDMAEMA$_m$ from PCL_n-Br macroinitiator; ^{1}H NMR recorded in DMSO-d_6 and $CDCl_3$of purified copolymers; SEC chromatograms of the copolymers using THF as eluent (1 mL/min) or DMAc as eluent (1 mL/min); Z-potential distributions of PCL-P(PEGMA), PCL-PGMA and PCL-PDMAEMA recorded at 25 °C, pH 7.4, and Z-potential distribution of PCL-PDMAEMA recorded at 25 °C, pH 5; cumulative DEX release profile from PCL-P(PEGMA), PCL-PGMA, and PCL-PDMAEMA NPs in PBS pH 7.4, 37 °C and sink conditions; parameters of KP and PS models obtained fitting the experimental release profile of DEX from PCL-P(PEGMA), PCL-PGMA, and PCL-PDMAEMA NPs in PBS at pH 7.4, 37 °C and sink conditions; IR spectra of pristine AC-HA hydrogel; DLS size distribution curve of PCL-PGMA NPs in PBS after microwave treatment for 1 min at 80 °C; tan(δ), evaluated as the ration between G'' and G', from rheological analysis of pristine AC-HA hydrogel, and AC-HA hydrogels encapsulating PCL-P(PEGMA), PCL-PGMA, and PCL-PDMAEMA NPs; G' and G'' of AC-HA pristine hydrogel from the frequency sweep test (at a fixed shear strain of 0.3%, within the linear viscoelastic region, assessed from the amplitude sweep test); representative SEM micrographs of lyophilized pristine AC-HA hydrogel, AC-HA hydrogel containing PCL-P(PEGMA) NPs, AC-HA hydrogel containing PCL-PGMA NPs, and AC-HA hydrogel containing PCL-PDMAEMA NPs; pictures of RhB-labeled NPs loaded into the hydrogel matrix; parameters of KP and PS models obtained fitting the experimental release profile of PCL-P(PEGMA), PCL-PGMA, and PCL-PDMAEMA NPs, encapsulated with physical, chemical, and ionic embedding procedures, from the composite hydrogel in PBS at pH 7.4, 37 °C under sink conditions; parameters of KP and PS models obtained fitting the experimental release profile of DEX from of PCL-P(PEGMA), PCL-PGMA, and PCL-PDMAEMA NPs-hydrogel systems, encapsulated with physical, chemical, and ionic encapsulation procedures; parameters of KP and PS models obtained fitting the experimental release profile of BSA from hydrogels embedding the three different NPs considered, encapsulated with physical, chemical and ionic embedding procedures; fluorescence microscopy images of the cells treated with 70% MeOH v/v mixed with culture medium (dead) and 100% culture medium (live); fraction of TNF-α and IL-6 released after 24 h from treatment with free DEX, or with DEX-loaded NPs-hydrogels composites (DOCX)

■ AUTHOR INFORMATION

Corresponding Authors

Filippo Rossi – *Department of Chemistry, Materials and Chemical Engineering "Giulio Natta", Politecnico di Milano, Via Edoardo Bassini 6, Milan 20133, Italy;* orcid.org/0000-0003-2665-120X; Email: filippo.rossi@polimi.it

Francesco Cellesi – *Department of Chemistry, Materials and Chemical Engineering "Giulio Natta", Politecnico di Milano, Via Edoardo Bassini 6, Milan 20133, Italy;* orcid.org/0000-0001-6106-9317; Email: francesco.cellesi@polimi.it

Authors

Alessandro Molinelli – *Department of Chemistry, Materials and Chemical Engineering "Giulio Natta", Politecnico di Milano, Via Edoardo Bassini 6, Milan 20133, Italy;* orcid.org/0000-0001-9230-9360

Ilaria Porello – *Department of Chemistry, Materials and Chemical Engineering "Giulio Natta", Politecnico di Milano, Via Edoardo Bassini 6, Milan 20133, Italy;* orcid.org/0009-0008-2129-3582

Francesco Briatico Vangosa – *Department of Chemistry, Materials and Chemical Engineering "Giulio Natta", Politecnico di Milano, Via Edoardo Bassini 6, Milan 20133, Italy;* orcid.org/0000-0002-7088-1064

Lara Longobardi – *Division of Rheumatology, Allergy and Immunology and Thurston Arthritis Research Center, University of North Carolina at Chapel Hill, Chapel Hill, North Carolina 27599, United States*

Richard F. Loeser – *Division of Rheumatology, Allergy and Immunology and Thurston Arthritis Research Center, University of North Carolina at Chapel Hill, Chapel Hill, North Carolina 27599, United States*

Complete contact information is available at: https://pubs.acs.org/doi/10.1021/acsbiomaterials.6c00470

Author Contributions

†A.M. and I.P. contributed equally to this work. A.M. and I.P.: Conceptualization, Data curation, Investigation, Methodology, Writing – original draft, Writing – review & editing. F.B.V., L.L., and R.F.L.: Methodology, Writing – review & editing. F.C. and F.R.: Funding acquisition, Supervision, Conceptualization, Data curation, Writing – review & editing.

Notes

The authors declare no competing financial interest.

■ ACKNOWLEDGEMENTS

The authors acknowledge partial financial support from the European Union's Horizon 2020 Research and Innovation

Programme under the Marie Sklodowska-Curie Grant Agreement No. 872648 (RISE-2019 "MEPHOS").

REFERENCES

(1) Lacroce, E.; Bianchi, L.; Polito, L.; Korganbayev, S.; Molinelli, A.; Sacchetti, A.; Saccomandi, P.; Rossi, F. On the Role of Polymeric Hydrogels in the Thermal Response of Gold Nanorods under NIR Laser Irradiation. *Nanoscale Adv.* **2023**, *5* (24), 6870–6879.

(2) Pham, D. T.; Navesit, K.; Wiwatkunupakarn, L.; Chomchalao, P.; Tiyaboonchai, W. Nanoparticles-Hydrogel Composites: A Promising Innovative System for Local Antimicrobial Applications. *J. Drug Delivery Sci. Technol.* **2023**, *89*, No. 105055.

(3) Choi, C. E.; Chakraborty, A.; Coyle, A.; Shamiya, Y.; Paul, A. Contact-Free Remote Manipulation of Hydrogel Properties Using Light-Triggerable Nanoparticles: A Materials Science Perspective for Biomedical Applications. *Adv. Healthc. Mater.* **2022**, *11* (8), No. 2102088.

(4) Baseeruddin Alvi, S.; P S, R.; Begum, N.; Jogdand, A. B.; Veeresh, B.; Rengan, A. K. In Situ Nanotransformable Hydrogel for Chemo-Photothermal Therapy of Localized Tumors and Targeted Therapy of Highly Metastatic Tumors. *ACS Appl. Mater. Interfaces* **2021**, *13* (47), 55862–55878.

(5) Yan, B.; Boyer, J. C.; Habault, D.; Branda, N. R.; Zhao, Y. Near Infrared Light Triggered Release of Biomacromolecules from Hydrogels Loaded with Upconversion Nanoparticles. *J. Am. Chem. Soc.* **2012**, *134* (40), 16558–16561.

(6) Ren, Y.; Li, X.; Han, B.; Zhao, N.; Mu, M.; Wang, C.; Du, Y.; Wang, Y.; Tong, A.; Liu, Y.; Zhou, L.; You, C.; Guo, G. Improved Anti-Colorectal Carcinomatosis Effect of Tannic Acid Co-Loaded with Oxaliplatin in Nanoparticles Encapsulated in Thermosensitive Hydrogel. *Eur. J. Pharm. Sci.* **2019**, *128*, 279–289.

(7) Nunes, D.; Andrade, S.; Ramalho, M. J.; Loureiro, J. A.; Pereira, M. C. Polymeric Nanoparticles-Loaded Hydrogels for Biomedical Applications: A Systematic Review on In Vivo Findings. *Polymers* **2022**, *14*, No. 1010.

(8) Zhao, H.; Liu, M.; Zhang, Y.; Yin, J.; Pei, R. Nanocomposite Hydrogels for Tissue Engineering Applications. *Nanoscale* **2020**, *12*, 14976–14995.

(9) Fan, Y.; Han, Q.; Li, H.; Cai, X.; Dyett, B.; Qiao, R.; Drummond, C. J.; Thang, S. H.; Zhai, J. Recent Developments in Nanoparticle-Hydrogel Hybrid Materials for Controlled Release. *Adv. Sci* **2025**, *12*, No. e07209.

(10) Li, C.; Obireddy, S. R.; Lai, W. F. Preparation and Use of Nanogels as Carriers of Drugs. *Drug Delivery* **2021**, *28* (1), 1594–1602.

(11) Xu, Y.; Zhu, H.; Denduluri, A.; Ou, Y.; Erkamp, N. A.; Qi, R.; Shen, Y.; Knowles, T. P. J. Recent Advances in Microgels: From Biomolecules to Functionality. *Small* **2022**, *18*, No. 2200180.

(12) Molinelli, A.; Schirato, A.; Moretti, L.; Della Valle, G.; Maiuri, M.; Rossi, F. Last Advances on Hydrogel Nanoparticles Composites in Medicine: An Overview with Focus on Gold Nanoparticles. *ChemNanoMat* **2024**, *10* (6), No. e202300584.

(13) Choi, W.; Kohane, D. S. Hybrid Nanoparticle-Hydrogel Systems for Drug Delivery Depots and Other Biomedical Applications. *ACS Nano* **2024**, 22780–22792.

(14) Egorikhina, M. N.; Timofeeva, L. B.; Linkova, D. D.; Rubtsova, Y. P.; Bugrova, M. L.; Charykova, I. N.; Ryabkov, M. G.; Kobyakova, I. I.; Farafontova, E. A.; Aleynik, D. Y. Biocompatibility Study of Hydrogel Biopolymer Scaffold with Encapsulated Mesenchymal Stem Cells. *Polymers* **2023**, *15* (6), No. 1337.

(15) Pillai, J. J.; Thulasidasan, A. K. T.; Anto, R. J.; Chithralekha, D. N.; Narayanan, A.; Kumar, G. S. V. Folic Acid Conjugated Cross-Linked Acrylic Polymer (FA-CLAP) Hydrogel for Site Specific Delivery of Hydrophobic Drugs to Cancer Cells. *J. Nanobiotechnol.* **2014**, *12* (1), No. 25.

(16) Chirizzi, C.; Gorini, F.; Porello, I.; Malferrari, M.; Becconi, M.; D'Arrigo, E.; Falciani, F.; Coschina, E.; Rapino, S.; Perrone, A. M.; De Iaco, P.; Metrangolo, P.; Baldelli Bombelli, F.; Ravegnini, G.; Cellesi, F. Hierarchical Paclitaxel Encapsulation in Microbead-Embedded Microparticles for Sustained Ovarian Cancer Therapy. *Int. J. Pharm.* **2025**, *683*, No. 125993.

(17) Porello, I.; Stucchi, F.; Sbaruffati, G.; Cellesi, F. Tailoring Copolymer Architectures and Macromolecular Interactions for Enhanced Nanotherapeutic Delivery: A Design-by-Architecture Approach. *Eur. Polym. J.* **2024**, *220*, No. 113455.

(18) Porello, I.; Stucchi, F.; Guarini, R.; Sbaruffati, G.; Cellesi, F. TCEP-Enabled Click Modification of Glycidyl-Bearing Polymers with Biorelevant Sulfhydryl Molecules: Toward Chemoselective Bioconjugation Strategies. *Biomacromolecules* **2025**, *28*, 5269–5286.

(19) Celentano, W.; Pizzocri, M.; Moncalvo, F.; Pessina, F.; Matteoli, M.; Cellesi, F.; Passoni, L. Functional Poly(ϵ-Caprolactone)/Poly(Ethylene Glycol) Copolymers with Complex Topologies for Doxorubicin Delivery to a Proteinase-Rich Tumor Environment. *ACS Appl. Polym. Mater.* **2022**, *4* (11), 8043–8056.

(20) Celentano, W.; Ordanini, S.; Bruni, R.; Marocco, L.; Medaglia, P.; Rossi, A.; Buzzaccaro, S.; Cellesi, F. Complex Poly(ε-Caprolactone)/Poly(Ethylene Glycol) Copolymer Architectures and Their Effects on Nanoparticle Self-Assembly and Drug Nanoencapsulation. *Eur. Polym. J.* **2021**, *144*, No. 110226.

(21) Jiang, Y.; Krishnan, N.; Heo, J.; Fang, R. H.; Zhang, L. Nanoparticle–Hydrogel Superstructures for Biomedical Applications. *J. Controlled Release* **2020**, *324*, 505–521.

(22) Lavrador, P.; Esteves, M. R.; Gaspar, V. M.; Mano, J. F. Stimuli-Responsive Nanocomposite Hydrogels for Biomedical Applications. *Adv. Funct. Mater.* **2021**, *31*, No. 2005941.

(23) Correa, S.; Grosskopf, A. K.; Klich, J. H.; Lopez Hernandez, H.; Appel, E. A. Injectable Liposome-Based Supramolecular Hydrogels for the Programmable Release of Multiple Protein Drugs. *Matter* **2022**, *5* (6), 1816–1838.

(24) Rossi, F.; Perale, G.; Storti, G.; Masi, M. A Library of Tunable Agarose Carbomer-Based Hydrogels for Tissue Engineering Applications: The Role of Cross-Linkers. *J. Appl. Polym. Sci.* **2012**, *123* (4), 2211–2221.

(25) Rossi, F.; Ferrari, R.; Castiglione, F.; Mele, A.; Perale, G.; Moscatelli, D. Polymer Hydrogel Functionalized with Biodegradable Nanoparticles as Composite System for Controlled Drug Delivery. *Nanotechnology* **2015**, *26* (1), No. 015602.

(26) Rossi, F.; Ferrari, R.; Papa, S.; Moscatelli, D.; Casalini, T.; Forloni, G.; Perale, G.; Veglianese, P. Tunable Hydrogel-Nanoparticles Release System for Sustained Combination Therapies in the Spinal Cord. *Colloids Surf., B* **2013**, *108*, 169–177.

(27) Molinelli, A.; Guacaneme Sánchez, J.; Schirato, A.; Briatico Vangosa, F.; Maiuri, M.; Rossi, F. Microwave Synthesis of Gold Nanoparticles in Poly(Ethylene Glycol)-Based Hydrogels for Drug Delivery. *ACS Appl. Nano Mater.* **2026**, *9* (11), 5067–5083.

(28) Bellotti, E.; Schilling, A. L.; Little, S. R.; Decuzzi, P. Injectable Thermoresponsive Hydrogels as Drug Delivery System for the Treatment of Central Nervous System Disorders: A Review. *J. Controlled Release* **2021**, *329*, 16–35.

(29) Porello, I.; Cellesi, F. Intracellular Delivery of Therapeutic Proteins. New Advancements and Future Directions. *Front. Bioeng. and Biotechnol.* **2023**, *11*, No. 1211798.

(30) Varanko, A.; Saha, S.; Chilkoti, A. Recent Trends in Protein and Peptide-Based Biomaterials for Advanced Drug Delivery. *Adv. Drug Delivery Rev.* **2020**, *156*, 133–187.

(31) Ogay, V.; Mun, E. A.; Kudaibergen, G.; Baidarbekov, M.; Kassymbek, K.; Zharkinbekov, Z.; Saparov, A. Progress and Prospects of Polymer-Based Drug Delivery Systems for Bone Tissue Regeneration. *Polymers* **2020**, *12*, 1–25.

(32) Roth, G. A.; Gale, E. C.; Alcantara-Hernandez, M.; Luo, W.; Axpe, E.; Verma, R.; Yin, Q.; Yu, A. C.; Hernandez, H. L.; Maikawa, C. L.; Smith, A. A. A.; Davis, M. M.; Pulendran, B.; Idoyaga, J.; Appel, E. A. Injectable Hydrogels for Sustained Codelivery of Subunit Vaccines Enhance Humoral Immunity. *ACS Cent. Sci.* **2020**, *6* (10), 1800–1812.

(33) Øvrebø, Ø.; Giorgi, Z.; De Lauretis, A.; Vanoli, V.; Castiglione, F.; Briatico-Vangosa, F.; Ma, Q.; Perale, G.; Haugen, H. J.; Rossi, F. Characterisation and Biocompatibility of Crosslinked Hyaluronic Acid

https://doi.org/10.1021/acsbiomaterials.6c00470
ACS Biomater. Sci. Eng. XXXX, XXX, XXX–XXX

with BDDE and PEGDE for Clinical Applications. *React. Funct. Polym.* **2024**, *200*, No. 105920.
(34) Appel, E. A.; Tibbitt, M. W.; Webber, M. J.; Mattix, B. A.; Veiseh, O.; Langer, R. Self-Assembled Hydrogels Utilizing Polymer-Nanoparticle Interactions. *Nat. Commun.* **2015**, *6*, No. 6295.
(35) Dong, X.; Liang, J.; Yang, A.; Qian, Z.; Kong, D.; Lv, F. Fluorescence Imaging Guided CpG Nanoparticles-Loaded IR820-Hydrogel for Synergistic Photothermal Immunotherapy. *Biomaterials* **2019**, *209*, 111–125.
(36) Abune, L.; Wang, Y. Affinity Hydrogels for Protein Delivery. *Trends in Pharmacol. Sci.* **2021**, *42*, 300–312.
(37) Di Francesco, M.; Primavera, R.; Romanelli, D.; Palomba, R.; Pereira, R. C.; Catelani, T.; Celia, C.; Di Marzio, L.; Fresta, M.; Di Mascolo, D.; Decuzzi, P. Hierarchical Microplates as Drug Depots with Controlled Geometry, Rigidity, and Therapeutic Efficacy. *ACS Appl. Mater. Interfaces* **2018**, *10* (11), 9280–9289.
(38) Di Francesco, M.; Bedingfield, S. K.; Di Francesco, V.; Colazo, J. M.; Yu, F.; Ceseracciu, L.; Bellotti, E.; Di Mascolo, D.; Ferreira, M.; Himmel, L. E.; Duvall, C.; Decuzzi, P. Shape-Defined MicroPlates for the Sustained Intra-Articular Release of Dexamethasone in the Management of Overload-Induced Osteoarthritis. *ACS Appl. Mater. Interfaces* **2021**, *13* (27), 31379–31392.
(39) Liu, S.; Zhang, C.; Zhou, Y.; Zhang, F.; Duan, X.; Liu, Y.; Zhao, X.; Liu, J.; Shuai, X.; Wang, J.; Cao, Z. MRI-Visible Mesoporous Polydopamine Nanoparticles with Enhanced Antioxidant Capacity for Osteoarthritis Therapy. *Biomaterials* **2023**, *295*, No. 122030.
(40) Li, G.; Liu, S.; Chen, Y.; Zhao, J.; Xu, H.; Weng, J.; Yu, F.; Xiong, A.; Udduttula, A.; Wang, D.; Liu, P.; Chen, Y.; Zeng, H. An Injectable Liposome-Anchored Teriparatide Incorporated Gallic Acid-Grafted Gelatin Hydrogel for Osteoarthritis Treatment. *Nat. Commun.* **2023**, *14* (1), No. 3159.
(41) Willcockson, H.; Greco, A.; Fragassi, A.; Palomba, R.; Kwon, K.; Ozkan, H.; Bartlett, S. T.; Loeser, R. F.; Decuzzi, P.; Longobardi, L. Sustained Release of Exogeneous Fetuin-A from Hyaluronic Acid Microplates Decreases Joint Degeneration, Synovial Hyperplasia and Muscle Damage in a Murine Post-Traumatic Osteoarthritis Model. *Arthritis Res. Ther.* **2025**, *27* (1), No. 178.
(42) Marrero - Berrios, I.; Salter, S. E.; Hirday, R.; Rabolli, C. P.; Tan, A.; Hung, C. T.; Schloss, R. S.; Yarmush, M. L. In Vitro Inflammatory Multi-Cellular Model of Osteoarthritis. *Osteoarthris Cartilage Open* **2024**, *6* (1), No. 100432.
(43) Pizzetti, F.; Maspes, A.; Rossetti, A.; Rossi, F. The Addition of Hyaluronic Acid in Chemical Hydrogels Can Tune the Physical Properties and Degradability. *Eur. Polym. J.* **2021**, *161*, No. 110843.
(44) Faivre, J.; Pigweh, A. I.; Iehl, J.; Maffert, P.; Goekjian, P.; Bourdon, F. Crosslinking Hyaluronic Acid Soft-Tissue Fillers: Current Status and Perspectives from an Industrial Point of View. *Expert Rev. Med. Devices* **2021**, *18*, 1175–1187.
(45) Coryell, P. R.; Hardy, P. B.; Chubinskaya, S.; Pearce, K. H.; Loeser, R. F. A Novel Small Molecule Screening Assay Using Normal Human Chondrocytes toward Osteoarthritis Drug Discovery. *Plos One* **2024**, *19* (11), No. e0308647.
(46) Loeser, R. F.; Pacione, C. A.; Chubinskaya, S. The Combination of Insulin-like Growth Factor 1 and Osteogenic Protein 1 Promotes Increased Survival of and Matrix Synthesis by Normal and Osteoarthritic Human Articular Chondrocytes. *Arthritis Rheum.* **2003**, *48* (8), 2188–2196.
(47) Muehleman, C.; Bareither, D.; Huch, K.; Cole, A. A.; Kuettner, K. E. Prevalence of Degenerative Morphological Changes in the Joints of the Lower Extremity. *Osteoarthritis Cartilage* **1997**, *5* (1), 23–37.
(48) Wood, S. T.; Long, D. L.; Reisz, J. A.; Yammani, R. R.; Burke, E. A.; Klomsiri, C.; Poole, L. B.; Furdui, C. M.; Loeser, R. F. Cysteine-Mediated Redox Regulation of Cell Signaling in Chondrocytes Stimulated with Fibronectin Fragments. *Arthritis Rheumatol.* **2016**, *68* (1), 117–126.
(49) Miao, M. Z.; Lee, J. S.; Yamada, K. M.; Loeser, R. F. Integrin Signalling in Joint Development, Homeostasis and Osteoarthritis. *Nat. Rev. Rheumatol.* **2024**, *20* (8), 492–509.
(50) Moncalvo, F.; Lacroce, E.; Franzoni, G.; Altomare, A.; Fasoli, E.; Aldini, G.; Sacchetti, A.; Cellesi, F. Protein-Friendly Atom Transfer Radical Polymerisation of Glycerol(Monomethacrylate) in Buffer Solution for the Synthesis of a New Class of Polymer Bioconjugates. *React. Funct. Polym.* **2022**, *175*, No. 105264.
(51) Bruni, R.; Possenti, P.; Bordignon, C.; Li, M.; Ordanini, S.; Messa, P.; Rastaldi, M. P.; Cellesi, F. Ultrasmall Polymeric Nanocarriers for Drug Delivery to Podocytes in Kidney Glomerulus. *J. Controlled Release* **2017**, *255*, 94–107.
(52) Yu, H.; Huang, C.; Kong, X.; Ma, J.; Ren, P.; Chen, J.; Zhang, X.; Luo, H.; Chen, G. Nanoarchitectonics of Cartilage-Targeting Hydrogel Microspheres with Reactive Oxygen Species Responsiveness for the Repair of Osteoarthritis. *ACS Appl. Mater. Interfaces* **2022**, *14* (36), 40711–40723.
(53) Lehtola, T.; Nummenmaa, E.; Tuure, L.; Hämäläinen, M.; Nieminen, R. M.; Moilanen, T.; Pemmari, A.; Moilanen, E. Dexamethasone Attenuates the Expression of MMP-13 in Chondrocytes through MKP-1. *Int. J. Mol. Sci.* **2022**, *23* (7), No. 3880.
(54) Ordanini, S.; Celentano, W.; Bernardi, A.; Cellesi, F. Mannosylated Brush Copolymers Based on Poly(Ethylene Glycol) and Poly(ε-Caprolactone) as Multivalent Lectin-Binding Nanomaterials. *Beilstein J. Nanotechnol.* **2019**, *10*, 2192–2206.
(55) Molinelli, A.; Bianchi, L.; Lacroce, E.; Giorgi, Z.; Polito, L.; De Luigi, A.; Lopriore, F.; Briatico Vangosa, F.; Bigini, P.; Saccomandi, P.; Rossi, F. Design and Characterization of Gold Nanorod Hyaluronic Acid Hydrogel Nanocomposites for NIR Photothermally Assisted Drug Delivery. *Gels* **2026**, *12* (1), 88.
(56) Cowman, M. K.; Lee, H.-G.; Schwertfeger, K. L.; McCarthy, J. B.; Turley, E. A. The Content and Size of Hyaluronan in Biological Fluids and Tissues. *Front. Immunol.* **2015**, *6*, No. 261.
(57) Petit, N.; Chang, Y. J.; Lobianco, F. A.; Hodgkinson, T.; Browne, S. Hyaluronic Acid as a Versatile Building Block for the Development of Biofunctional Hydrogels: In Vitro Models and Preclinical Innovations. *Mater. Today Bio* **2025**, *31*, No. 101596.
(58) Sauerová, P.; Pilgrová, T.; Pekař, M.; Hubálek Valbáčová, M. Hyaluronic Acid in Complexes with Surfactants: The Efficient Tool for Reduction of the Cytotoxic Effect of Surfactants on Human Cell Types. *Int. J. Biol. Macromol.* **2017**, *103*, 1276–1284.
(59) Yoon, M. S.; Lee, J. M.; Jo, M. J.; Kang, S. J.; Yoo, M. K.; Park, S. Y.; Bong, S.; Park, C.-S.; Park, C.-W.; Kim, J.-S.; Han, S.-B.; Lee, H. J.; Shin, D. H. Dual-Drug Delivery Systems Using Hydrogel–Nanoparticle Composites: Recent Advances and Key Applications. *Gels* **2025**, *11* (7), No. 520.
(60) Rossi, F.; Veglianese, P.; Santoro, M.; Papa, S.; Rogora, C.; Dell'Oro, V.; Forloni, G.; Masi, M.; Perale, G. Sustained Delivery of Chondroitinase ABC from Hydrogel System. *J. Funct. Biomater.* **2012**, *3* (1), 199–208.
(61) Kang, Y.; Guan, Y.; Li, S. Innovative Hydrogel Solutions for Articular Cartilage Regeneration: A Comprehensive Review. *Int. j. surg.* **2024**, *110*, 7984–8001.
(62) Heo, D. N.; Kim, H. J.; Lee, D.; Kim, H.; Lee, S. J.; Lee, H. R.; Kwon, I. K.; Do, S. H. Comparison of Polysaccharides in Articular Cartilage Regeneration Associated with Chondrogenic and Autophagy-Related Gene Expression. *Int. J. Biol. Macromol.* **2020**, *146*, 922–930.
(63) Vanoli, V.; Delleani, S.; Casalegno, M.; Pizzetti, F.; Makvandi, P.; Haugen, H.; Mele, A.; Rossi, F.; Castiglione, F. Hyaluronic Acid-Based Hydrogels: Drug Diffusion Investigated by HR-MAS NMR and Release Kinetics. *Carbohydr. Polym.* **2023**, *301*, No. 120309.
(64) Herrada-Manchón, H.; Fernández, M. A.; Aguilar, E. Essential Guide to Hydrogel Rheology in Extrusion 3D Printing: How to Measure It and Why It Matters? *Gels* **2023**, *9*, No. 517.
(65) Porello, I.; Cellesi, F. Intracellular Delivery of Therapeutic Proteins. New Advancements and Future Directions. *Front. Bioeng. Biotechnol.* **2023**, *11*, No. 1211798.
(66) Fologea, D.; Ledden, B.; McNabb, D. S.; Li, J. Electrical Characterization of Protein Molecules by a Solid-State Nanopore. *Appl. Phys. Lett.* **2007**, *91* (5), 053901-1–053901-3.

https://doi.org/10.1021/acsbiomaterials.6c00470
ACS Biomater. Sci. Eng. XXXX, XXX, XXX–XXX

(67) Reed, K. S. M.; Ulici, V.; Kim, C.; Chubinskaya, S.; Loeser, R. F.; Phanstiel, D. H. Transcriptional Response of Human Articular Chondrocytes Treated with Fibronectin Fragments: An in Vitro Model of the Osteoarthritis Phenotype. *Osteoarthritis Cartilage* **2021**, *29* (2), 235–247.

(68) Forsyth, C. B.; Pulai, J.; Loeser, R. F. Fibronectin Fragments and Blocking Antibodies to A2β1 and A5β1 Integrins Stimulate Mitogen-Activated Protein Kinase Signaling and Increase Collagenase 3 (Matrix Metalloproteinase 13) Production by Human Articular Chondrocytes. *Arthritis Rheum.* **2002**, *46* (9), 2368–2376.

https://doi.org/10.1021/acsbiomaterials.6c00470
ACS Biomater. Sci. Eng. XXXX, XXX, XXX–XXX